Nanocomposite for Organic Pollutant Removal and Hydrogen Production through Photocatalysis

A Dissertation

Submitted for the partial fulfillment

of

the award of the degree of

MASTERS OF SCIENCE

in

CHEMISTRY

By

Bhavika Garg

(Reg. No. : 302202002)

Under the supervision of

Dr. SOUMEN BASU

Professor

Department of Chemistry and Biochemistry

Thapar Institute of Engineering and Technology

Patiala-147004, Punjab

July 2024

CERTIFICATE

This is to certify that the dissertation entitled ***"Nanocomposite for Organic Pollutant Removal and Hydrogen Production through Photocatalysis"*** being submitted by **Bhavika Garg** to the **Department of Chemistry and Biochemistry, Thapar Institute of Engineering and Technology, Patiala,** in partial fulfillment of the requirements for the award of the degree of **Master of Science in Chemistry,** is an authentic record of the work carried out by the candidate under my guidance and supervision. She has complied with all procedures for submitting this dissertation, which, as far as I know, meets the necessary standards.

There hasn't been any partial or complete submission of the dissertation's findings to another university or institute for the award of another degree or diploma.

Bhavika Garg

Date – 31/07/2024 **Bhavika Garg**

Place: TIET, Patiala **(302202002)**

It is certified that the aforementioned statement made by the student is correct to the best of my knowledge and belief.

S Basu P.

Dr. Soumen Basu

Professor

Department of Chemistry and Biochemistry

Thapar Institute of Engineering and Technology, Patiala.

CANDIDATE'S DECLARATION

I hereby declare that the dissertation entitled ***"Nanocomposite for Organic Pollutant Removal and Hydrogen Production through Photocatalysis "*** submitted in partialfulfillment of the requirements for the award of a degree in **Masters of Science in Chemistry** to the **Department of Chemistry and Biochemistry at the Thapar Institute of Engineering and Technology, Patiala** is a record of my work done under the supervision of **Dr. Soumen Basu**, Professor, Department of Chemistry and Biochemistry, Thapar Institute of Engineering and Technology. Additionally, none of the components of this dissertation have been submitted to another university for consideration for a different degree or diploma.

Bhavika Garg

Date: 31/07/2024
Place: TIET, Patiala

Bhavika Garg
(302202002)

ACKNOWLEDGEMENT

First and foremost, I want to express my gratitude to **God** for providing me with the strength and determination that I needed throughout the entire duration of this project.

I extend my deepest and sincerest appreciation to my project supervisor, **Dr. Soumen Basu,** Professor, Department of Chemistry and Biochemistry, Thapar Institute of Engineering and Technology, Patiala. His immense support, constant motivation, and invaluable guidance have been instrumental in completing my project. I am genuinely grateful for the privilege and honor of working under his constructive mentorship, which consistently steered me in the right direction.

I am immensely grateful to **Dr. Manmohan Chhibber,** Professor and Head of the Department of Chemistry and Biochemistry, for allowing me to work on this dissertation project. I would like to express my heartfelt appreciation to all the faculty and staff at DCBC for their guidance and support throughout this journey.

I am deeply grateful to **Mr. Pritam Hait** and **Ms. Palkaran** for their unwavering support, comprehensive understanding, and vast expertise. Their genuine sincerity, patience, and warm-hearted nature have been a constant source of inspiration. Their thoughtful suggestions, delivered with kindness and encouragement, have played a pivotal role in ensuring the smooth completion of this project.

I am filled with profound gratitude towards my lab seniors who consistently provided me with cooperative guidance, a friendly demeanor, and invaluable assistance throughout my project.

I express my obligation to the **Thapar Institute of Engineering and Technology & Department of Chemistry and Biochemistry** for generous funding and the essential infrastructure and research facilities that enabled me to conduct my experiments successfully.

Lastly, but of utmost importance, I am immensely thankful to my **parents, family, and friends**, who have showered me with unconditional love, priceless affection, heartfelt prayers, and constant support in every facet of my life.

Table of Contents

List of Figures

List of Tables

List of Schemes

List of Abbreviations

GCN	g-C_3N_4
SBS	Sb_2S_3
GS	g-C_3N_4/Sb_2S_3 nanocomposite
PANI	Polyaniline
RB19	Reactive Blue-19
TC	Tetracycline
XRD	X-Ray Diffraction
XPS	X-Ray Photoelectron Spectroscopy
FESEM	Field Emission Scanning Electron Microscopy
EDS	Energy-dispersive X-Ray Spectroscopy
PL	Photoluminescence Spectroscopy
BET	Brunauer–Emmett–Teller
UV-Vis	Ultraviolet-Visible
DRS	Diffuse Reflectance Spectroscopy
TOC	Total Organic Carbon
COD	Chemical Oxygen Demand
FT-IR	Fourier Transform Infrared Spectroscopy

eV	Electron Volt
λ_{max}	Absorption Maxima
wt.	Weight
m^2/g	Meter square per gram
nm	Nanometer
^{o}	Degree Celsius
mL	Milliliter
a.u.	Arbitrary Units
g/L	Gram per liter
h	Hours
min	Minutes
mg	Milligram
PCS	Porous Carbon Spheres

ABSTRACT

This study focuses on developing a g-C_3N_4/Sb_2S_3 heterojunction photocatalyst with different g-C_3N_4 to Sb_2S_3 weight ratios (1:1, 1:3, and 3:1) for degrading tetracycline (TC) pollutants. The 1:3 ratio (13GS) exhibited optimal photocatalytic performance, achieving 99% TC degradation under sunlight within 120 minutes, compared to 78.4% under visible light and 38% under UV light. The 13GS catalyst demonstrated strong reusability, maintaining 80% degradation efficiency after six cycles. Scavenger experiments identified hydroxyl radicals as crucial for TC degradation, with DMSO reducing activity by 30%. The photocatalyst also showed high hydrogen production with an apparent quantum efficiency (AQE) of 19.8% under standard conditions, and improved AQE in acidic (23%) and basic (22.7%) conditions, and with CH_3OH (23.2%). This g-C_3N_4/Sb_2S_3 heterojunction offers a promising solution for degrading toxic contaminants and has the potential for solar-powered applications.

Keywords: graphitic-carbon nitride/Antimony trisulfide; binary nanocomposite; photocatalysis, organic pollutant degradation; photocatalytic hydrogen evolution.

1.1 Basic frame

Water pollution has been identified as a major global concern due to fast population expansion and rapid industrialization of cities[1] [2]. Reports suggest that over 2 billion individuals are not getting safe water for drinking and that hundreds of thousands die every year from illnesses caused by water contamination [3]. Pharmaceutical pollutants like antibiotics are a significant hazard to freshwater ecosystems and humans because they discharge into many environmental resources, including soil, sediment, surface water, groundwater, and drinking water [4].

1.2 Tetracycline (TC) – A colorless pollutant

Aquaculture and veterinary care extensively use tetracycline (TC), a class of antibiotics. Most of them are eliminated in their unmetabolized parent form through feces and urine because of their low absorption[5]. Genetic transference and resistance to drugs by bacteria are two potential outcomes of TC presence in aquatic environments, which endangers aquatic life and human health[6]. The most significant environmental impact of antibiotics is the rise of bacteria resistant to all known drugs[7]. Consequently, both human and environmental health must eliminate TC antibiotic residues from the environment [8]. The structure of the tetracycline is shown in the **figure 1**.

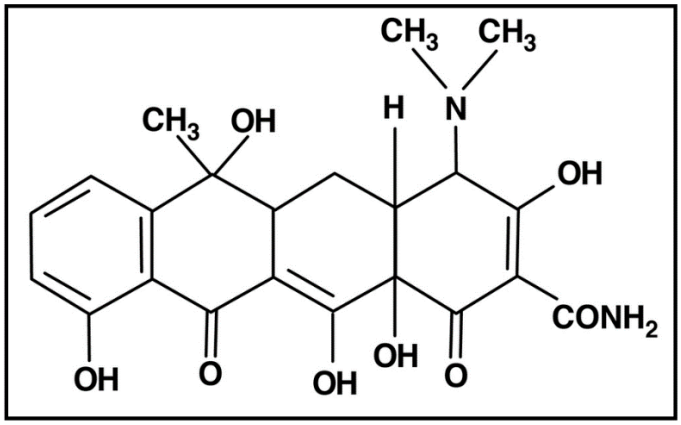

Figure 1 Structure of tetracycline antibiotic

1.3 Practices for wastewater treatment

Several methods have been explored for the removal of antibiotics and dyes from water, including ion exchange, anaerobic digestion, nanofiltration, adsorption, reverse osmosis, ultrafiltration, ozonation, semiconductor photocatalysis (alone and in combination with aerobic treatment), photo-Fenton, electrochemical oxidation, biological treatment with advanced oxidation processes, and many more[9][10][11][12][13][14][15][16][17][18]. At the very end of the treatment process, these approaches produce secondary pollutants, which in turn raise the pressure and temperature and diminish their efficacy [19]. For example, since bacteria are becoming more resistant to antibiotics, anaerobic biological treatment has not been able to remove antibiotic residue from wastewater adequately. This is because the antibiotics either do not degrade completely or adsorb to sludge[20]. In addition, conventional methods of wastewater treatment have a hard time removing TC and RB19 because of their insoluble molecular structure and poor biodegradability. Hence, we need an affordable, highly effective, and green technique to remove antibiotics like TC and dyes like RB19 from water.

1.4 Photocatalytic degradation and some heterojunction photocatalysts

Photocatalytic degradation is a green and sustainable method that uses UV-visible light to degrade the pollutants. Additionally, it does not produce any harmful byproducts. Organic pollutants are broken down into smaller molecules or degraded into CO_2 and H_2O[21] using this approach and this method can be used to treat a wide range of pollutants. For photocatalysis to work, creating an ideal photocatalyst that becomes active when exposed to UV-visible light is necessary. So, there is a need to create an optimum photocatalyst with a low energy band gap, large surface area, and lesser rate of recombination of charge carriers.

Graphitic carbon nitride (g-C_3N_4), a polymeric semiconductor, has lately garnered considerable attention in the domain of photocatalysis[22][23]. With a band gap energy of 3.0 eV and visible region activity, it is a frequently utilized material in photocatalysis thanks to its strong physicochemical stability, quick and simple synthesis, "earth-ample" character, and the fact that it captures the structure of its electronic band[24]. Because of its high rate of electron-hole recombination and low light absorption propensity, the effectiveness of its photocatalytic degradation is not very high. To minimize the recombination of charges and capture charge

carriers, another photoactive material should be attached with g-C_3N_4 to create a heterojunction[25].

Antimony trichloride (Sb_2S_3) is an exceptional photocatalyst that efficiently absorbs sunlight due to its tiny energy band gap of around 1.66 eV. Its exceptional electrochemical, photoelectronic, and optical properties are noteworthy, as are its non-carcinogenic qualities. Lithium-ion batteries, Gas detectors, photoelectronic gadgets, solar power cells, near-infrared photonic devices, and many more applications might benefit greatly from Sb_2S_3 nano-materials [26][27]. The Sb_2S_3/α-Ag_2WO_4 heterojunction was able to obtain a degradation efficiency of 91.23% of the methylene blue dye within 60 minutes of being illuminated by visible light [28]. The degradation rate for rhodamine B dye was 77.65% and for thiamethoxam, it was 62% when exposed to sunshine for 150 minutes through a Sb_2S_3/PCS (porous carbon spheres) heterojunction [29]. Using hydrothermal techniques, Peng et al. synthesized MoS_2/g-C_3N_4 hybrids with a 60% degrading efficiency for organic pollutant degradation[30]. The maximum degradation rate of 89% was achieved in 60 minutes by Meng et al. when they created g-C_3N_4 nanorods loaded with WO_3-based photocatalysts for the removal of rhodamine B dye[31]. To the best of our knowledge, nobody to date has tried to use g-C_3N_4/Sb_2S_3 nanocomposite. Although pure g-C_3N_4 and Sb_2S_3 have been created and combined with other materials before, this study takes a novel approach by investigating the photocatalytic use of these two together. The synergy resulting from combining Sb_2S_3 and g-C_3N_4 has demonstrated significant promise in enhancing the photocatalytic activities of g-C_3N_4.

1.5 Present work

In this study, various mole ratios of g-C_3N_4/Sb_2S_3 nanocomposite were synthesized by the hydrothermal technique. An experiment for photocatalytic degradation was conducted to evaluate the efficacy of the synthesized photocatalyst against the harmful and colorless pollutant, TC, utilizing natural sunlight as the light source. Various tests were undertaken, encompassing scavenger studies, pH effects, kinetic analysis, photocatalyst dose manipulation, and reusability analysis. The degradation efficacies of TC were tested under various conditions of light. Additionally, the photocatalyst's effectiveness was evaluated by contrasting its degradation efficiency to that of the commonly available TiO_2-P25. GC–MS was used to examine the produced

disintegrated products. Additional mineralization investigations have also been carried out. Finally, the suggested photocatalytic mechanism was presented.

1.6 Thesis objective

Our fundamental approach involved the synthesis of such nanocomposite that aimed at effectively eliminating toxic organic pollutants present in wastewater. This was achieved by incorporating Sb_2S_3 onto g-C_3N_4 resulting in the formation of a highly efficient heterojunction nanocomposite for wastewater treatment. The nanocomposite's structure and composition were meticulously analyzed using advanced techniques such as Brunauer–Emmett–Teller (BET) and X-ray Diffraction spectroscopy (XRD). The elemental oxidation state was thoroughly investigated through the application of X-ray photoelectron spectroscopy (XPS). To gain insight into its morphology, Field Emission Scanning Electron Microscopy (FESEM) was used. Furthermore, Photoluminescence spectroscopy (PL) enabled a comprehensive assessment of the nanocomposite's electronic properties, providing valuable insights into their efficiency. To comprehensively examine and compare the decomposition and adsorption ability of the photocatalysts, a range of studies were conducted. By meticulously analyzing these factors, a deeper understanding of the photocatalyst's performance and its response to different conditions was attained.

Previous research has successfully developed a range of nanocomposites utilizing g-C_3N_4, and Sb_2S_3, as core materials. These hybrid nanocomposites exhibit diverse structures, surface morphologies, and sizes, and have shown significant potential in various practical applications. These applications include the degradation of harmful organic pollutants, detection of hazardous heavy metal ions, hydrogen production, and enhancement of nitrification processes.

The combination of g-C_3N_4 with Sb_2S_3 in this nanocomposite has demonstrated notable efficiency in degrading antibiotics. Specifically, incorporating Sb_2S_3 onto the surface of g-C_3N_4 markedly improves the separation of charge carriers generated by light, which results in extended light absorption and enhanced photocatalytic performance.

Berekute et al. (2023) successfully developed a novel binary nanocomposite, P-g-C_3N_4/α-Bi_2O_3, using a hydrothermal-calcination method. The P-g-C_3N_4/α-Bi_2O_3 nanocomposite, with a 25 wt% composition, exhibited superior catalytic performance compared to its components in degrading 4-hydroxybenzophenone (4H-BP) and benzophenone-1 (BP-1). The enhanced photocatalytic efficiency of this nanocomposite is largely attributed to the formation of a heterojunction and improved light absorption, which significantly boost the separation and mobility of charge carriers generated by light. Under visible light, the nanocomposite achieved high degradation rates of 95% for BP-1 and 94% for 4H-BP[32].

In 2022, Xiao and colleagues successfully synthesized a Sb_2S_3-$ZnIn_2S_4$ heterostructure using a one-step hydrothermal method. This innovative structure features $ZnIn_2S_4$ nanosheets growing uniformly on Sb_2S_3 nanorods, forming a closely bonded interface between the two materials. The resulting heterostructure significantly improves several key photocatalytic properties: it enhances light absorption, increases the surface area, shortens the electron diffusion path, and facilitates the efficient migration and separation of photoexcited charge carriers. The optimized Sb_2S_3-$ZnIn_2S_4$ heterostructure demonstrated an impressive photocatalytic hydrogen production rate of 1685.14 μmol/g/h. In addition to its exceptional hydrogen generation performance, this photocatalyst exhibited remarkable efficiency in degrading pollutants. It achieved an 85.36% removal rate of Tetracycline hydrochloride. Furthermore, it displayed substantial degradation capabilities for

Oxytetracycline (80.52%) and 2-mercaptobenzothiazole (84.30%) under visible light over approximately 140 minutes. These results underscore the significant potential of this nanocomposite catalyst for applications in environmental remediation, offering an effective solution for the treatment of various contaminants[33].

When we compare our findings with the studies summarized in **Table 1**, it is clear that our catalyst not only surpasses the performance of those previously reported but also exhibits remarkable effectiveness even at lower doses. The integration of g-C_3N_4 with Sb_2S_3 emerges as an exceptionally effective combination. This blend has demonstrated superior performance in our research, highlighting its potential for achieving better results compared to other catalysts studied in the past.

Table 1 List of various g-C_3N_4, Sb_2S_3, CuBTC, and PANI-based nanocomposites reported in the literature

Photocatalyst	Reaction time (min)	Catalytic efficiency (%)	Reference
$BiVO_4$ /Sb_2S_3	120	88.7	[27]
Sb_2S_3 /$ZnIn_2S_4$	140	85.36	[33]
Ag_2WO_4 /Sb_2S_3	180	53.06	[34]
Fe doped g-C_3N_4/MoS_2	120	81.4	[35]
MoS_2/C_3N_4	180	74	[36]
g-C_3N_4 / Sb_2S_3	120	99	[37]

3.1 Materials and methodology

3.1.1 Chemicals and materials

Urea, antimony trichloride ($SbCl_3$), thioacetamide (C_2H_5NS), and tartaric acid ($C_4H_6O_6$) were acquired from Loba Chemie. The TC powder used in this study was obtained from Sigma Aldrich. The solutions were prepared using ultrapure double-distilled water. Pure reagents were used without any adulteration.

3.1.2 Synthesis of graphitic carbon nitride (g-C_3N_4)

Initially, urea (40g) was placed into a silica crucible. It was dissolved in 100 mL of water and was then subjected to recrystallization by heating it in an oven at a temperature of 90ºC. The recrystallized urea was then scratched, covered with aluminum foil, and put in the muffle furnace for heating. A temperature of 550 ℃ was achieved and maintained for two hours after being increased to 10 ℃ each minute. Yellow-brown colored precipitates of g-C_3N_4 were obtained which were then ground with a mortar pestle and were identified as GCN [38].

3.1.3 Synthesis of antimony trisulfide (Sb_2S_3)

Antimony trichloride (0.3650 g), tartaric acid (1.5 g), and thioacetamide (0.24 g) were combined in a beaker with 80 ml of water. The resulting mixture was hydrothermally treated for 8 hours at 180ºC after being agitated at room temperature for one night. The next step was to dry the product in an oven set at 40ºC after three washes with water and two with ethanol. Ultimately, the black powder of Sb_2S_3 was obtained and subsequently determined to be SBS [27].

3.1.4 Synthesis of g-C_3N_4/Sb_2S_3 composites

In a beaker, specific quantities of g-C_3N_4 were measured (200 mg, 600 mg, and 200 mg for ratios of 1:1, 3:1, and 1:3, respectively). Additionally, predetermined amounts of antimony trichloride ($SbCl_3$) (0.3650 g, 0.3650 g, and 1.095 g), tartaric acid (1.5 g, 1.5 g, and 4.5 g), and thioacetamide (0.24 g, 0.24 g, and 0.72 g) were added as the precursors for Sb_2S_3 along with 80 mL of water. The resulting solution was agitated at room temperature for one night and subsequently subjected to hydrothermal treatment at 180°C for 8 hours. Following this, the ratios were subjected to centrifugation, washed three times using water and twice with ethanol, and finally dried in a hot air oven at 40°C. In this way, composites were prepared and were named 11GS, 31GS, and 13GS

respectively. The synthesis scheme with real images of the g-C_3N_4/Sb_2S_3 hybrid is illustrated in **Scheme 1**.

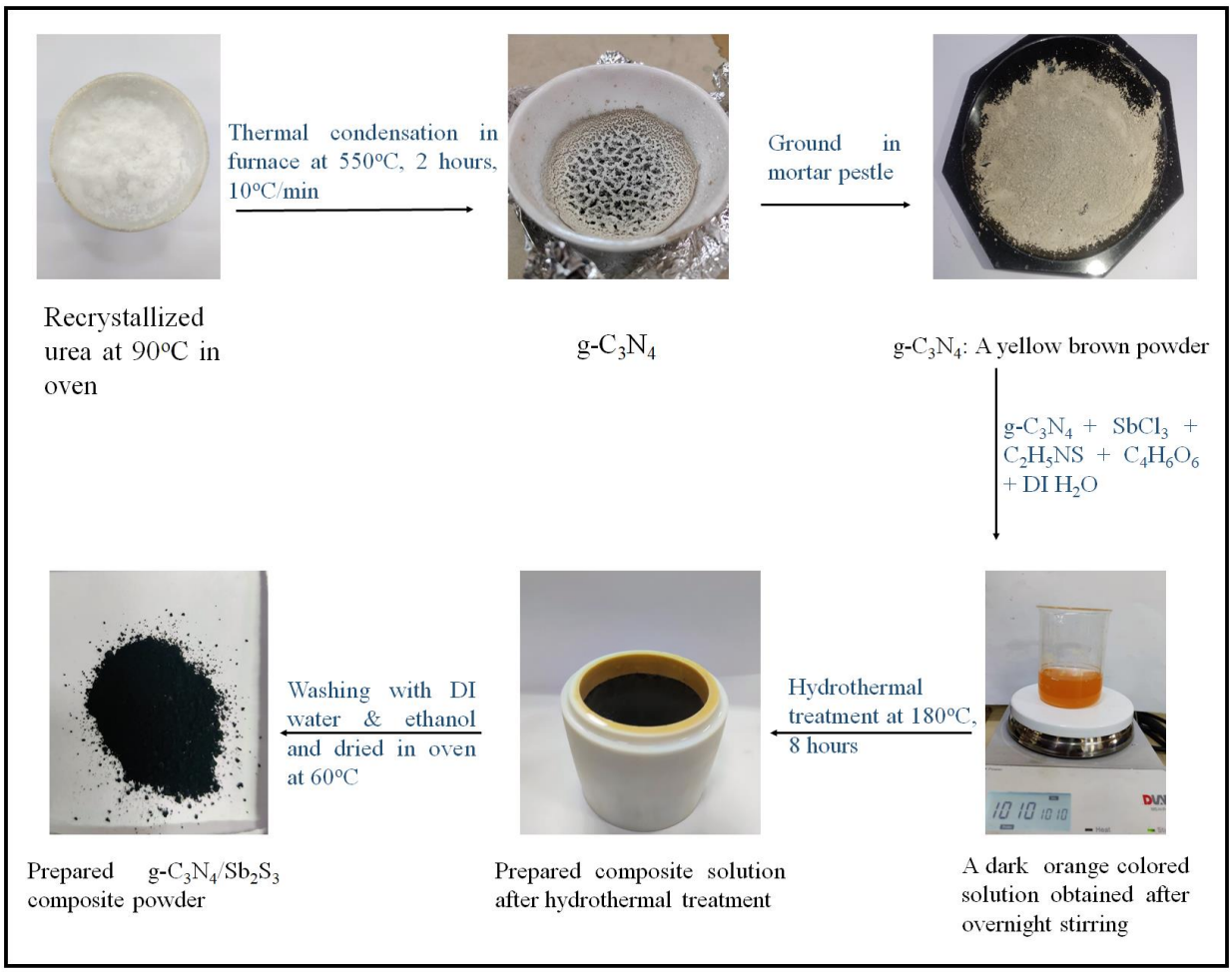

Scheme 1 Synthesis of g-C_3N_4/Sb_2S_3 photocatalyst

3.2 Results and discussion

3.2.1 XRD analysis

The X-ray diffraction (XRD) patterns of the nanocomposites, as well as the bare photocatalysts, are present in **Fig 2**.

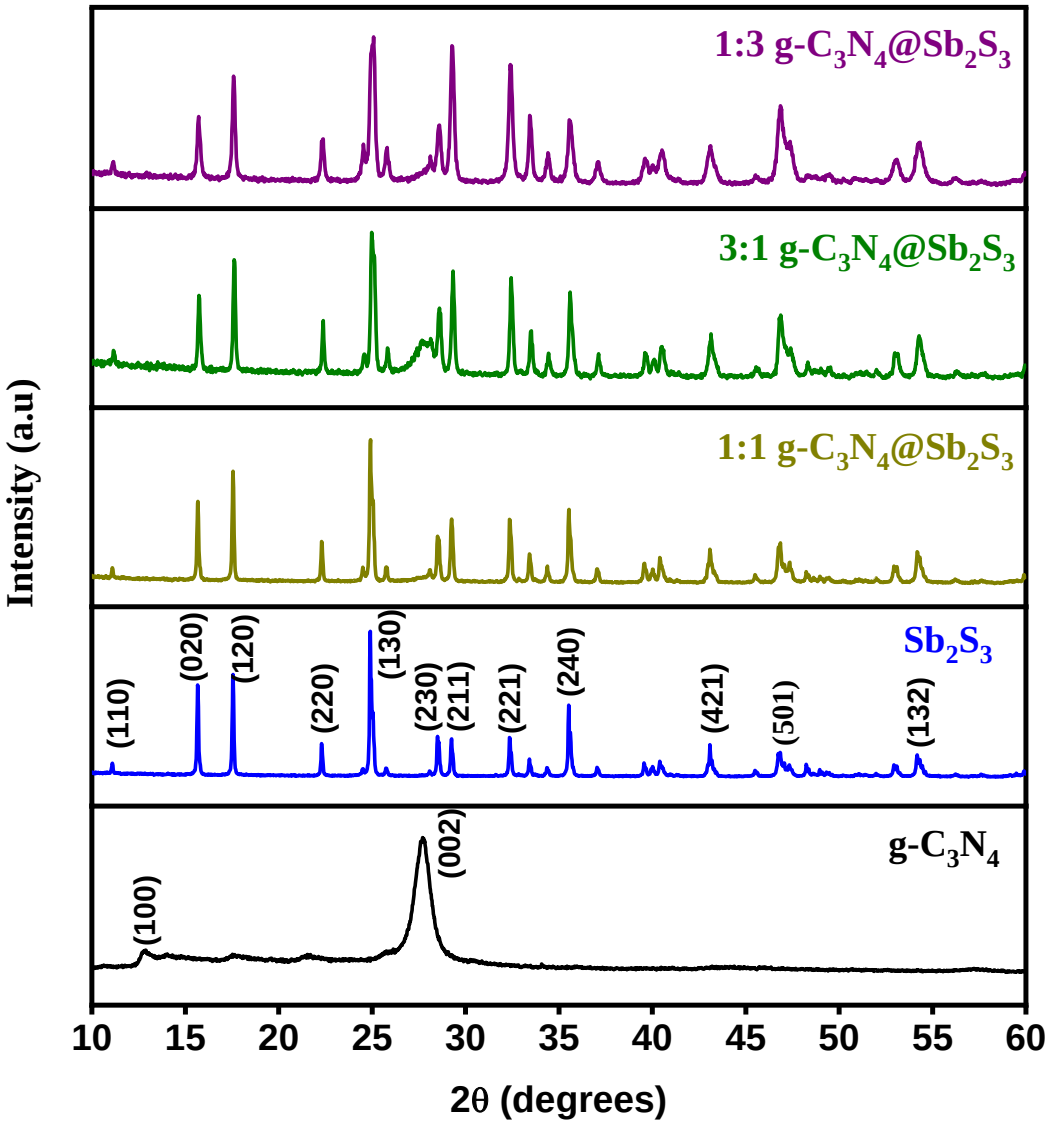

Figure 2 XRD pattern of pure GCN, SBS, 11GS, 31GS, and 13GS composites

The GCN crystal planes are responsible for the peaks seen at 2θ ~12.7° (100) and 28° (002) (JCPDS 87-1526). As per the JCPDS card number 00-006-0474, the diffraction peaks of SBS at 2θ ~ 11.04° (110), 15.62° (020), 17.58° (120), 22.27° (220), 24.88° (130), 28.4° (230), 29.26° (211), 32.42°

(221), 35.5^{o} (240), 43.1^{o} (421), 46.8^{o} (501), and 54.2^{o} (132) are observed, which confirms the orthorhombic arrangement of SBS. The photocatalysts probably have a crystalline structure since there are clear sharp peaks. The composites also showed both kinds of peaks. It appears that the composites were successfully fabricated because no further impurity peak was seen. The very nonexistent peak displacement further showed the great degree of purity and two-phase composition of the binary heterojunction photocatalysts.

3.2.2 XPS studies

The X-ray photoelectron spectroscopy (XPS) technology was used to analyze the elemental composition, core electron binding energy, and oxidation states of the elements. Metal ions with different binding energies can be identified by XPS as having spin-orbit divided into two different states. The original composite survey spectra are shown in **Fig 3(a).** Based on the peaks, the main components of the 13GS composite are nitrogen, sulfur, carbon, and antimony. Deconvolution was performed using the least-square Gaussian-fit model. Carbon spectra (C 1s) with deconvoluted peaks at binding energies of 284.6 eV, 286.7 eV, and 288.1 eV (**Fig 3(b)**) can be attributed to graphitic carbon or C—N [39], C≡N, and N=C—N_2 of striazine ring (C_3N_3) units or heptazine (C_6H_7) units respectively [40]. The nitrogen (N 1s) spectra display peaks at 398.7 eV, 399.2 eV, and 400.7 eV (**Fig 3(c)**) corresponding to pyridine N, pyrrolic N, and graphitic N respectively [41]. **Fig 3(d)** illustrates 4 peaks of antimony (Sb 3d), out of which the peaks observed at 539.2 eV and 529.8 eV are due to Sb $3d_{3/2}$ and Sb $3d_{5/2}$ respectively [42]. The peaks at 540.2 eV and 530.8 eV are due to Sb $3d_{3/2}$ and Sb $3d_{5/2}$ of Sb_2O_3 due to the presence of Sb_2O_3 impurity in the Sb_2S_3 sample[43]. **Fig 3(e)** depicts two peaks of sulfur (S 2p) at binding energies 161.5 eV and 162.6 eV corresponding to S $2p_{3/2}$ and S $2p_{1/2}$ respectively [44].

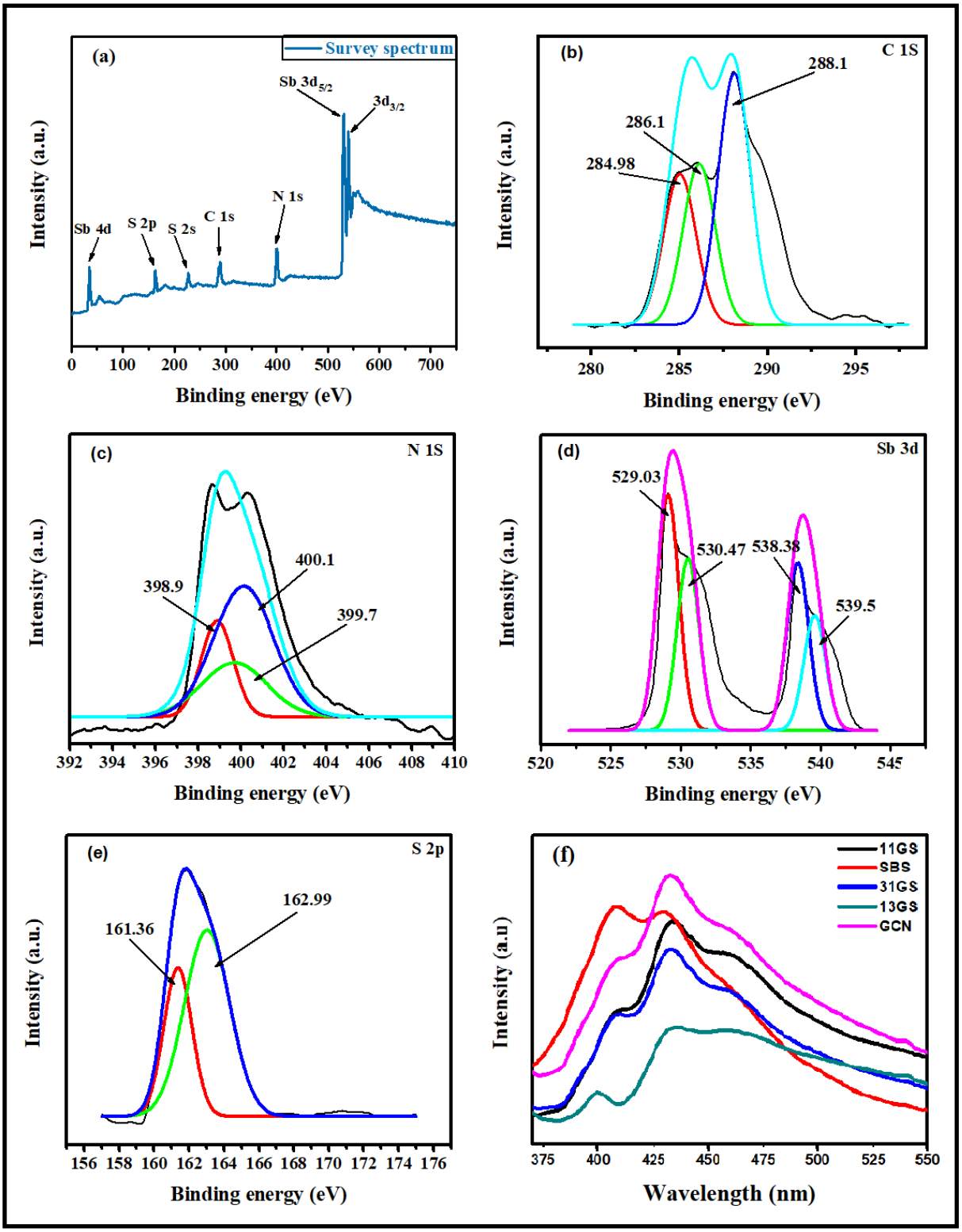

Figure 3 XPS spectra of 13GS, (a) survey spectra, (b) C 1s, (c) N 1s, (d) Sb 3d, (e) S 2p, and (f) photoluminescence spectra of photocatalysts

3.2.3 Photoluminescence studies

To analyze the catalytic efficiency, photoluminescence spectra were taken of bare materials as well as the composites which are shown in **Fig 3(f)**. Effective charge segregation, a large capacity for conveying charge carriers, and a low rate of assimilation are the characteristics of an excellent photocatalyst. A straightforward method to measure the rate of recombination of the charge carriers is the emission intensity of the PL signal. Diminutive emission enhances photocatalytic activity and charge transfer efficiency since this means that the electron and hole reintegration rate is lowered [47]. These spectroscopic measurements were conducted with an excitation wavelength of 350 nm. Notably, the bare GCN and SBS materials exhibited significantly higher emission intensity than the composites, indicating a greater efficiency of the composites relative to the bulk materials. Among the various ratios tested, 13GS exhibited the lowest emission intensity, indicating the least recombination rate of charge carriers and consequently demonstrating the highest catalytic efficiency. The reduced photoluminescence intensity can be attributed to the formation of a heterojunction and the synergistic interaction between the two distinct components, which aids in effectively separating the charge carriers.

3.2.4 Surface properties

We used nitrogen sorption experiments to check the synthesized material's surface area characteristics and pore size distribution. **Figures 4** and **5**, show that the photocatalysts are mesoporous, as shown by their type-IV nitrogen adsorption-desorption curve. By utilizing the BJH plot, the pore sizes may be determined. The specific surface area, pore diameter, and mean pore volume values are summarized in **Table 2**. The 13GS hetero-composite had the largest specific surface area compared to all the other synthesized nanocomposites. Because of their wide surface area, heterojunction photocatalysts enhance charge migration by bringing the two components into better interfacial contact. With so many surface-active sites exposed, the photocatalytic efficiency is boosted, allowing for the adsorption of a huge number of contaminants [45].

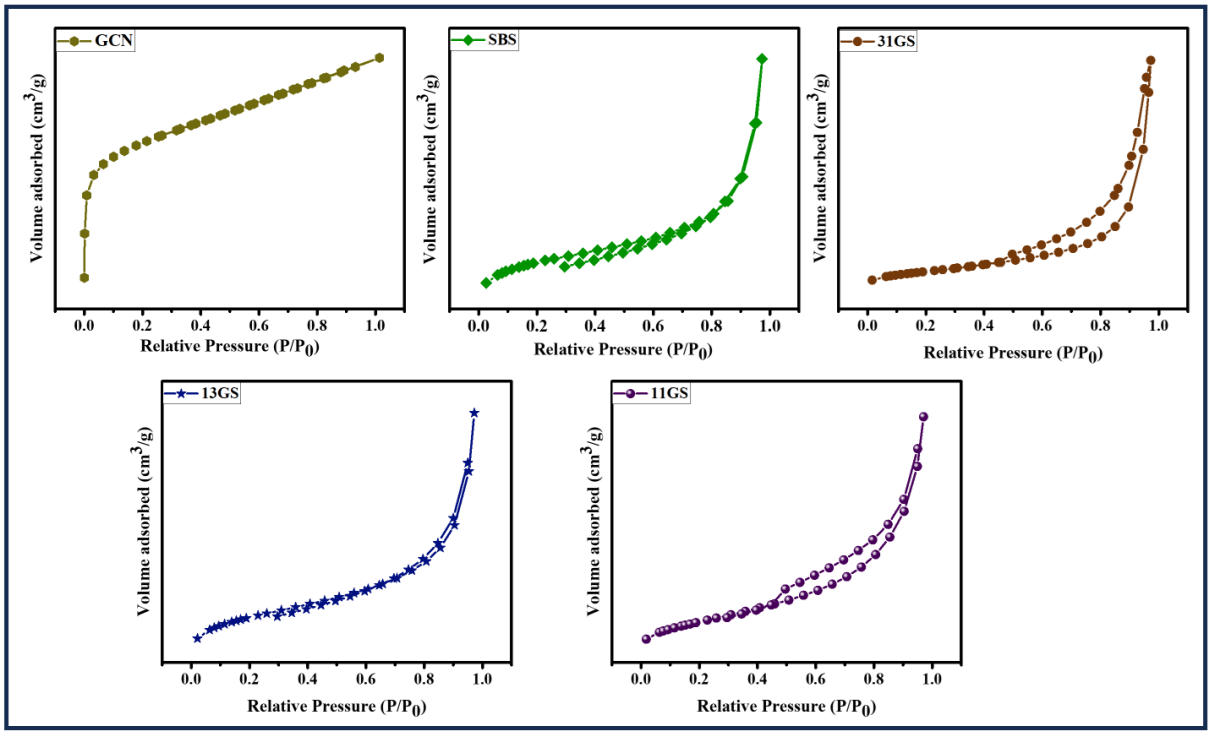

Figure 4 BET isotherms

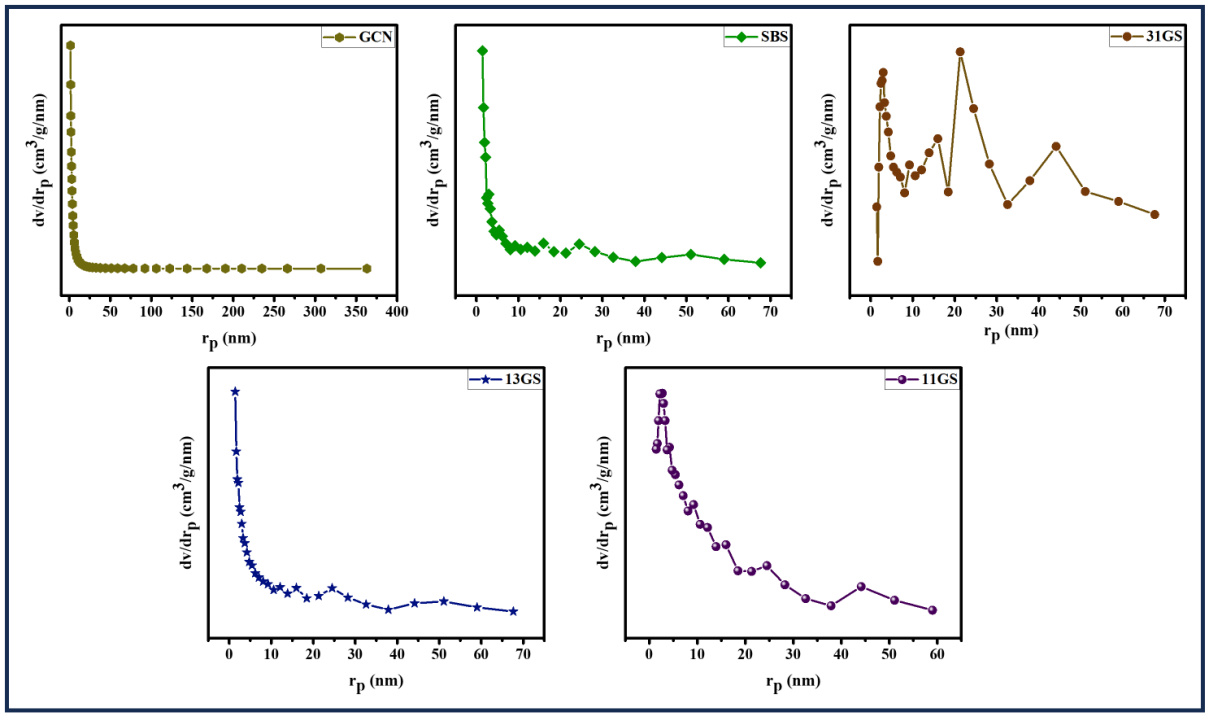

Figure 5 BJH plot to determine the pore size of the synthesized photocatalysts

Table 2 Surface characteristics of the synthesized photocatalysts

Sample	Pore diameter (nm)	Specific Surface Area (m^2 /g)	Mean Pore Volume (cm^3 /g)
g-C_3N_4	2.62	88.12	0.057
Sb_2S_3	8.81	1.56	0.003
1:1 g-C_3N_4@Sb_2S_3	10.18	2.65	0.006
3:1 g-C_3N_4@Sb_2S_3	9.16	1.49	0.003
1:3 g-C_3N_4@Sb_2S_3	18.19	5.08	0.023

3.2.5 Morphological characterization

To understand the morphological and structural features of the newly designed binary nanocomposite, FE-SEM analysis was carried out. **Fig 6** illustrates FESEM images of synthesized GCN, SBS, and 13GS composite. The results revealed that GCN showed a nano-sheet-like structure (**Fig 6(a)**), and SBS had nano-rods-like morphological characteristics (**Fig 6(b)**). However, the nanocomposite has both morphologies, indicating the effective formation of the heterojunction (**Fig 6(c)**). Furthermore, this dual shape provides a multitude of potential sites, which increases the catalyst's surface area and enhances the ability to adsorb pollutants and degrade them by photocatalysis [46]. The elemental distribution and composition of the photocatalyst were evaluated using EDS (**Fig 6(d)**). The synthesized nanocomposite was found to contain C, N, Sb, and S according to the EDS analysis. Figure **6(e)** shows the nanocomposite's elemental color mapping, which further guarantees the uniform distribution of all the components, which helps to boost the photocatalytic efficacy. The results show that the SBS is well dispersed onto GCN, which is a great quality of a heterojunction photocatalyst.

Fig. 7 displays the HRTEM images of the synthesized nanocomposite 13GS, revealing the presence of layered g-C_3N_4 sheets and Sb_2S_3 particles. In fig. **7**, two distinct types of lattice fringes can be observed, corresponding to the (020), and (002) planes with d-spacings of 0.566, and 0.0.319 nm, respectively. These fringes are associated with Sb_2S_3 ($2\Theta = 15.62°$), and g-C_3N_4 ($2\Theta = 28°$).

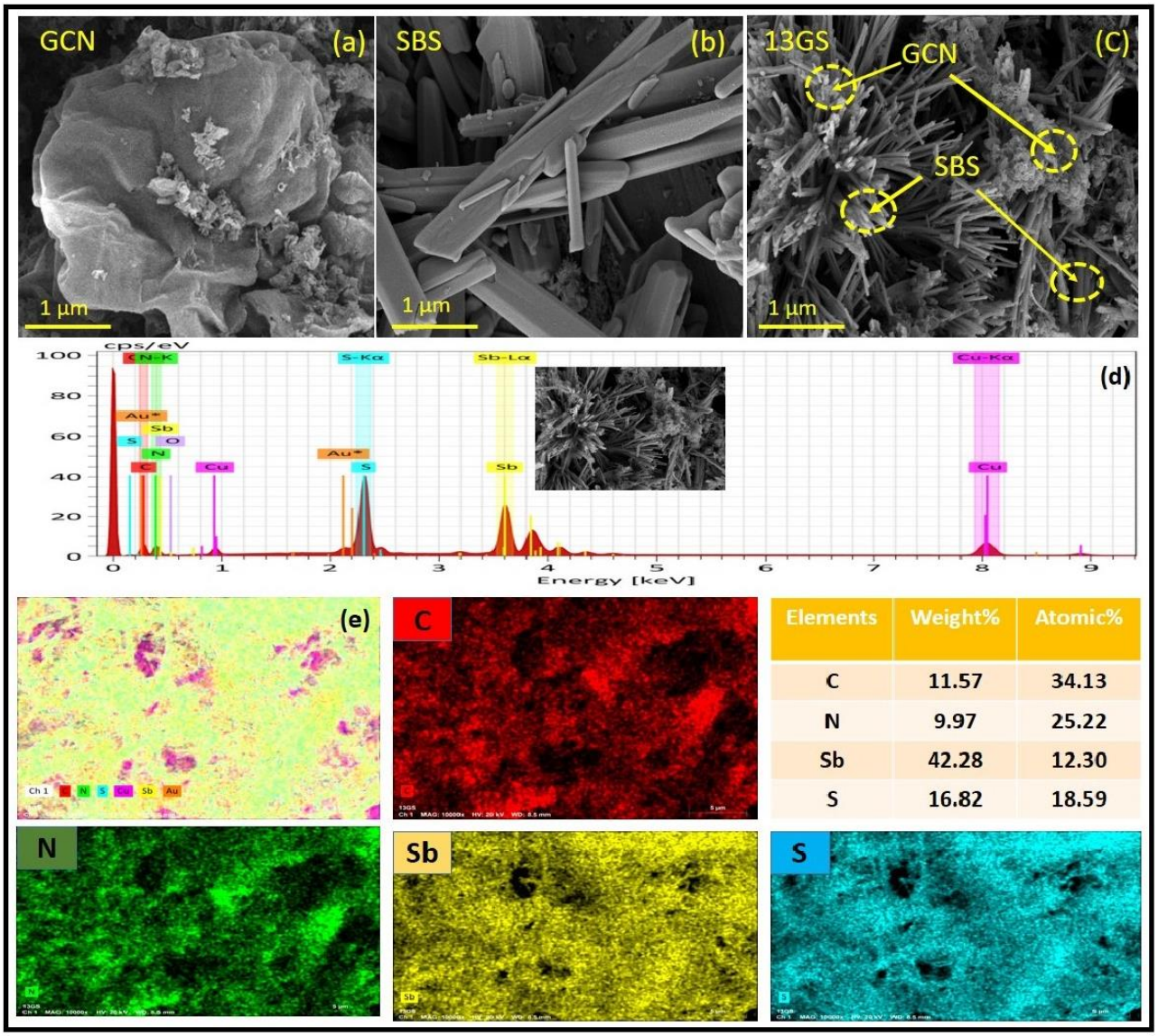

Elements	Weight%	Atomic%
C	11.57	34.13
N	9.97	25.22
Sb	42.28	12.30
S	16.82	18.59

Figure 6 FE-SEM images of (a) GCN, (b) SBS, (c) 13GS nanocomposite, (d) EDS spectrum of the 13GS nanocomposite with its corresponding FE-SEM image, and (e) elemental mapping of the 13GS nanocomposite

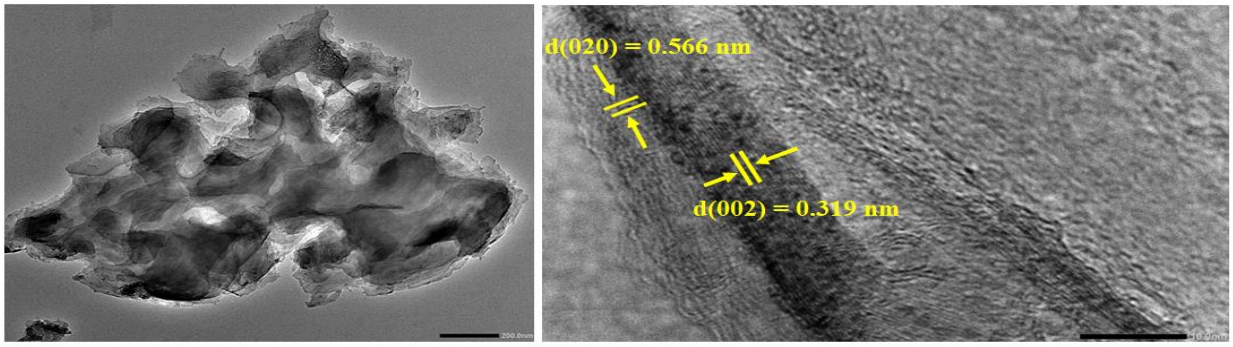

Figure 7 HRTEM images of 13GS

3.2.6 EIS measurements

EIS measurements were used to assess the charge transfer efficiency in Sb_2S_3, g-C_3N_4, and its nanocomposite. A smaller arc radius in the Nyquist plot typically signifies enhanced interfacial charge transport and improved charge separation. The arc radii observed followed this order: Sb_2S_3 > g-C_3N_4 > 13GS. **Fig. 8** shows that adding Sb_2S_3 and g-C_3N_4 co-catalysts reduced the arc radius, indicating lower electron transfer resistance and reduced electron-hole pair recombination, which improved interfacial charge carrier transport. The ternary 13GS composite had the smallest arc radius, reflecting its superior conductivity, faster charge migration, and better separation of photo induced carriers. These EIS findings align with the PL analysis, highlighting the ternary hybrid's 13GS crucial role in enhancing charge separation.

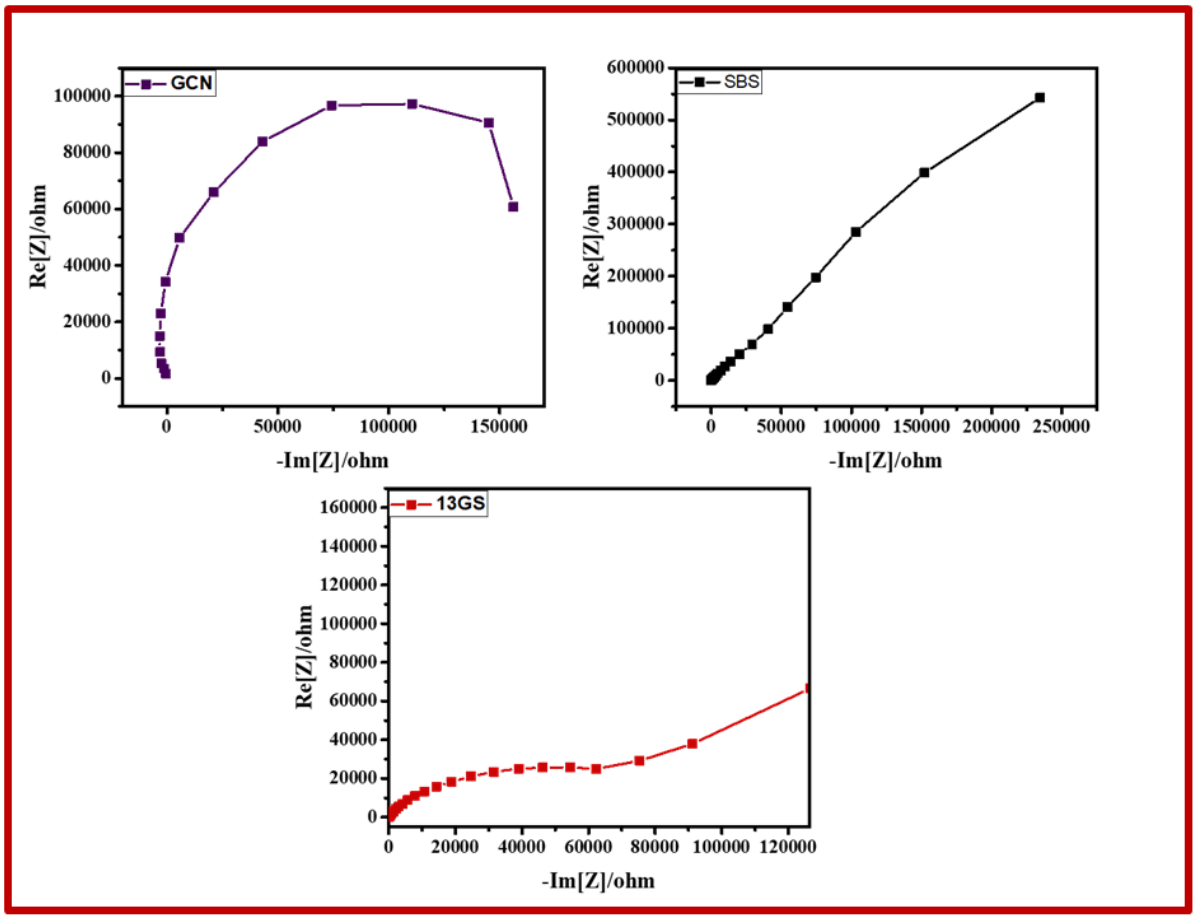

Figure 8 Impedance analysis

3.2.6 DRS studies

Both a small energy gap and high light absorption strength are necessary for a photocatalyst to be effective. The adsorption range and band gap were examined using UV-DRS. **Equation 1** below was used to get the Tauc plot, which allowed us to compute the band gap energy.

$$(\alpha h\nu)^{1/2} = h\nu - E_g \quad \textbf{(1)}$$

In this context, the absorption coefficient (α), Planck's constant (h), light frequency (ν), and band gap energy (E_g) are denoted, accordingly. From **Fig 9(a)**, it can be inferred that GCN shows maximum absorbance in the UV region but when its composites are made with SB, their absorbance increases in the visible region. The E_g values were ascertained by extending the Tauc plot to the x-axis, representing photon energy [4]. Consequently, as shown in **Fig 9(b)**, band gaps of 3.0 eV for GCN, 1.66 eV for SBS, 1.61 eV for 13GS, 1.68 eV for 31GS, and 1.65 eV for 11GS were determined, respectively. Based on these results, the 13GS composite is the best photocatalyst that can absorb visible light and has the lowest energy band gap.

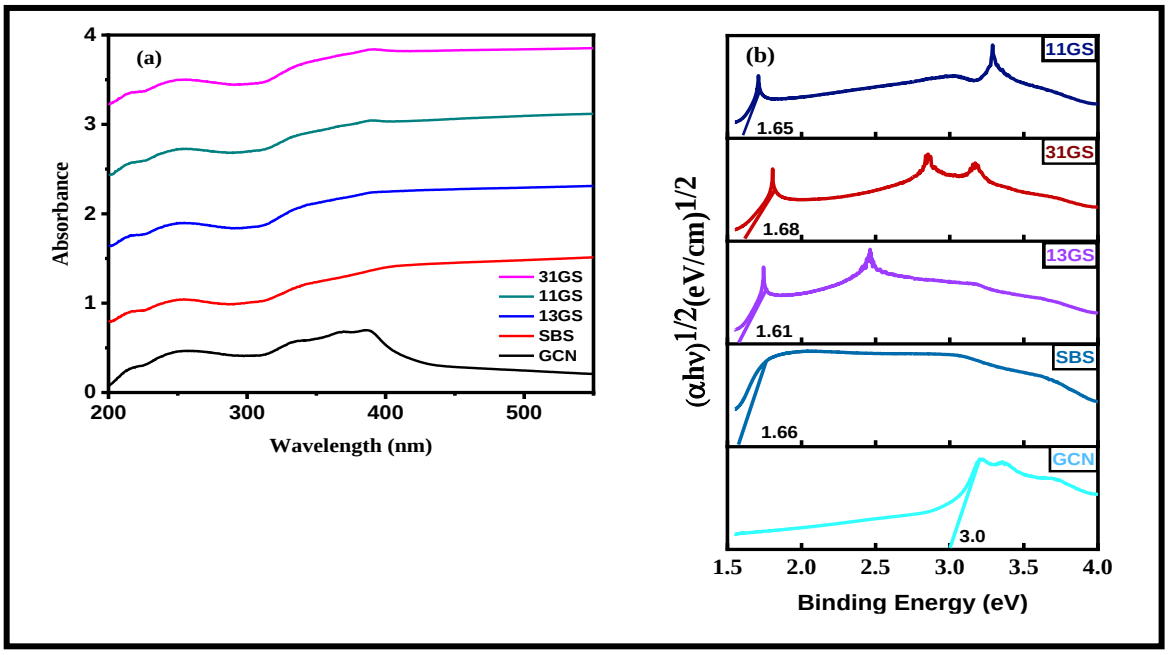

Figure 9 (a) UV-Visible DRS absorption spectra, and (b) the band gap energies of GCN, SBS, 13GS, 31GS, and 11GS

3.2.7 FTIR analysis

The FTIR Spectra of GCN, SBS, and their composites are shown in **Fig 10**. A wide peak at 3000-3300 cm^{-1} is seen in GCN, which is caused by the stretching vibration of the N—H bond. As for

the C—N and C≡N heterocycles, there is a strong band from 1200-1650 cm^{-1} with peaks at 1241, 1319, 1403, 1465, 1573, and 1634 cm^{-1}. The triazine unit's breathing mode is indicated by the peak at 810 cm^{-1} [48]. In SBS a peak at 673 cm^{-1} is observed due to Sb—S bond [29]. The nanocomposites exhibit absorption peaks corresponding to all these different functional groups, which are seen to undergo slight shifts in wavenumber. This observation confirms the successful synthesis of the nanocomposites.

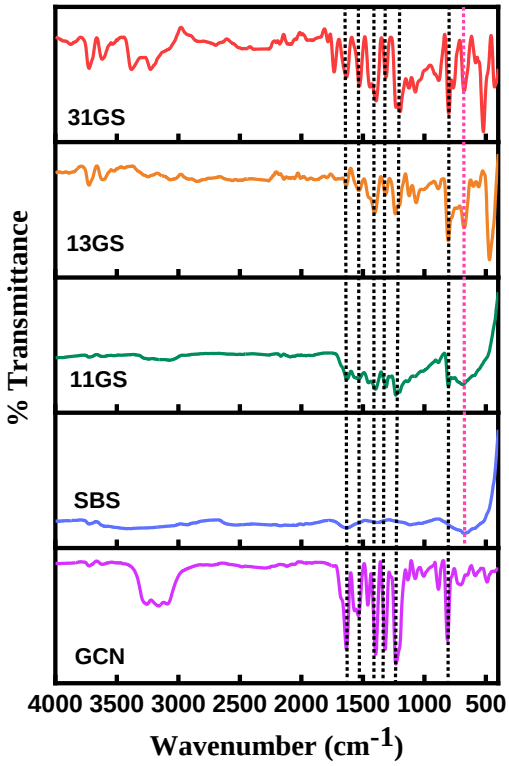

Figure 10 FTIR spectra of different as-synthesized photocatalysts

3.2.8 Photocatalytic activity

The photocatalytic efficacy of 13GS was assessed by degrading the contaminant Tetracycline (TC) using natural sunlight. In a subtropical environment in Patiala, India, at the Thapar Institute of Engineering & Technology, the photocatalysis experiment was carried out. A LICOR pyranometer measured the average solar radiation intensity, resulting in a value of 850 W/m^2. With an estimated intensity of 100 W/m^2, a 45 W compact fluorescent lamp (Philips) was used to illuminate the solution with visible light. A 100-watt mercury lamp emits light at a wavelength of 365 nm. The flux density of this lamp's light ranges from 66 to 68 watts per square meter and was

used to irradiate the solution with ultraviolet light. We constructed graphs with error bars that have a margin of error of roughly 5% after repeating the photocatalytic tests three times. The maximum absorption wavelengths (λ_{max}) were measured at 360 nm for TC when the absorbance spectra were checked regularly with a UV-visible spectrophotometer. The degradation efficiency was calculated using the **equation 2**.

$$\%\, Degradation = \frac{A_o - A_t}{A_o} \times\ 100 \quad \textbf{(2)}$$

In this context, % Degradation stands for degradation efficiency, A_0 for initial absorbance, and A_t for absorbance at time t. The photolysis experiment involved exposing a solution containing 10 mL of 5 ppm TC to sunshine for 120 minutes. The greatest degradation rate of 99% was observed in the presence of the 13GS photocatalyst. To determine the most effective catalyst dosage for the degradation of TC, from 0.1 g/L to 0.6 g/L, we tested various concentrations of the 13GS catalyst. (**Fig 11(a)**). Our findings revealed that the degradation efficiency improved notably as we increased the catalyst concentration from 0.1 g/L to 0.2 g/L. However, the efficiency plateaued beyond this point, and any further increase in catalyst concentration resulted in only marginal improvements. This phenomenon can be attributed to the rising opacity and enhanced dispersion of the dye solution at higher catalyst concentrations [49]. This can also be due to the deactivation of the active sites, resulting in a loss of their efficacy. We found that 0.2 g/L of the photocatalyst was a suitable concentration for future experiments. The experiment was carried out using a catalyst concentration of 0.2 g/L to determine the reaction kinetics. Firstly, the solution was stirred in darkness for 120 minutes to ensure optimal absorption of the dye. Subsequently, it was exposed to sunshine for 120 minutes to undergo photocatalytic degradation. To assess the effectiveness of the nanocomposite, a comparative experiment was conducted using GCN, SBS, TiO_2 (P25) (a commercially available photocatalyst), 11GS, 13GS, and 31GS. We computed the rate constant, (k) using the **equation 3**:

$$\ln \frac{C}{C_o} = -kt \quad \textbf{(3)}$$

Here, C_0 is the starting concentration, C is the concentration at time t, and k is the rate constant. From **Fig 11(b-c)** it can be concluded that the reaction followed pseudo-first-order kinetics. With a rate constant of 0.0304 min^{-1}, the 13GS composite outperformed the bare GCN (0.0075 min^{-1}),

SBS (0.0057 min^{-1}), and ratios of 31GS (0.0142 min^{-1}) and 11GS (0.0064 min^{-1}) in terms of efficiency. The degree of synergistic impact in the composites was evaluated by computing the synergy factor (R) using the **equation 4**:

$$R= \frac{K_{GCN+SBS}}{K_{GCN}+K_{SBS}} \quad \textbf{(4)}$$

Here $K_{GCN+SBS}$, $K_{GCN,}$ and K_{SBS} are the rate constants of 13GS binary composite, pure GCN, and pure SBS respectively. Results showed that 13GS composite showed the highest synergy factor that leads to maximum photocatalytic degradation efficiency. In **Table 3**, you can find the rate constants and synergy factors for all of the photocatalysts.

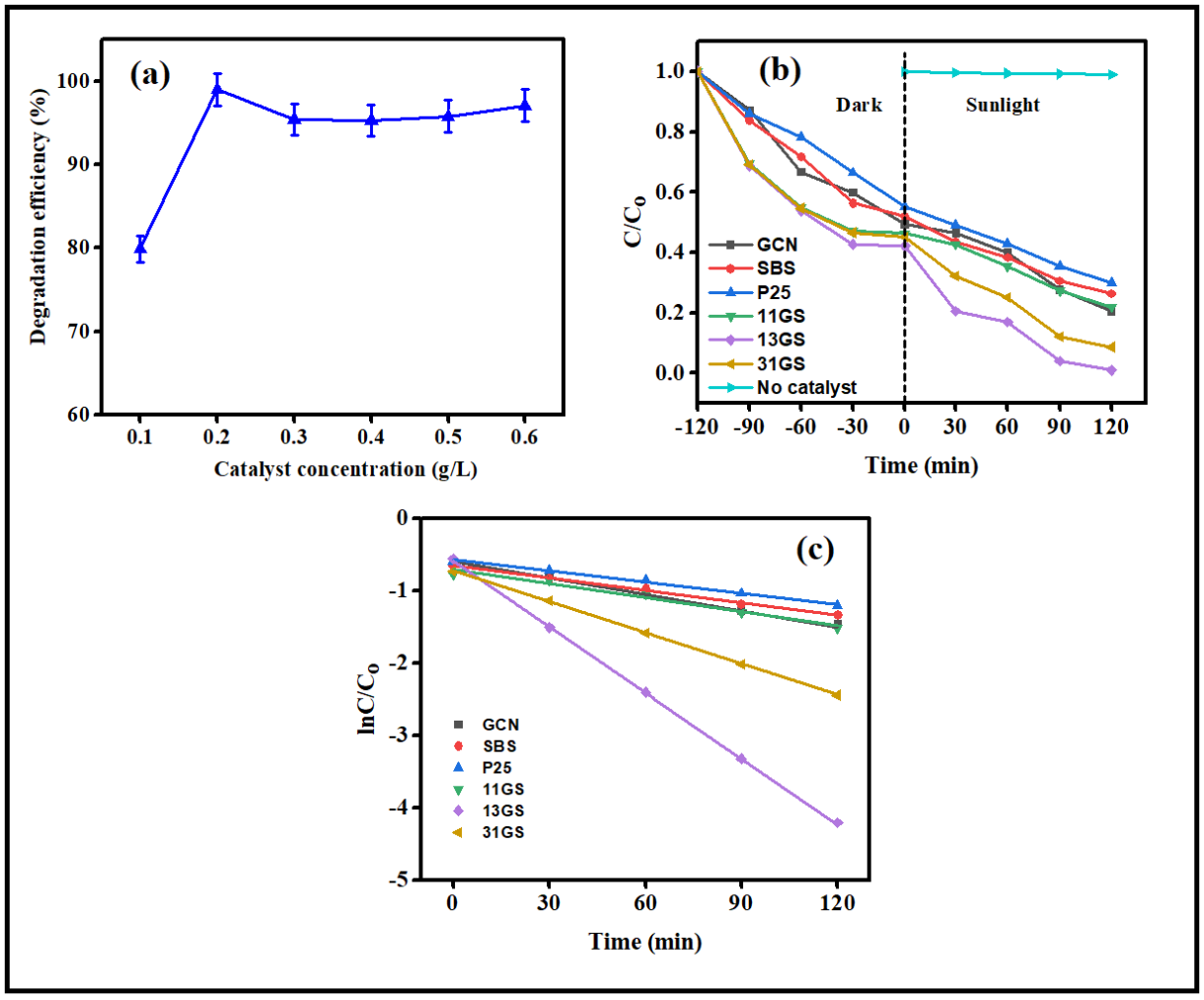

Figure 11 (a) Concentration impact of 13GS photocatalyst, (b) and (c) kinetics in degrading TC under controlled conditions (0.2 g/L catalyst, 10 mL dye solution, pH 7, and 120 minutes of sunshine irradiation)

Table 3 The synergy factors and degradation rate constants attained by photo-catalytic TC elimination

Material	Rate constant (min^{-1})	Synergy Factor (R)
TiO_2-P25	0.0051	-
g-C_3N_4	0.0075	-
Sb_2S_3	0.0057	-

1:1 g-C_3N_4@Sb_2S_3	0.0064	0.48
1:3g-C_3N_4@Sb_2S_3	0.0304	2.3
3:1 g-C_3N_4@Sb_2S_3	0.0142	1.07

3.2.9 Influence of light sources

Ideal conditions were used for comparative photocatalytic studies using different light sources, such as UV, visible, and natural daylight. Looking at **Figure 12** clearly shows that the TC degradation was 38% when exposed to UV light and 78.4% when exposed to visible light. The 13GS heterojunction photocatalyst attained a maximum elimination rate of 99% under natural sunlight. The results indicate that the created photocatalyst can efficiently break down the pollutant with the help of natural sunlight. Therefore, natural sunshine is more important for the degradation of pollutants compared to artificial light sources.

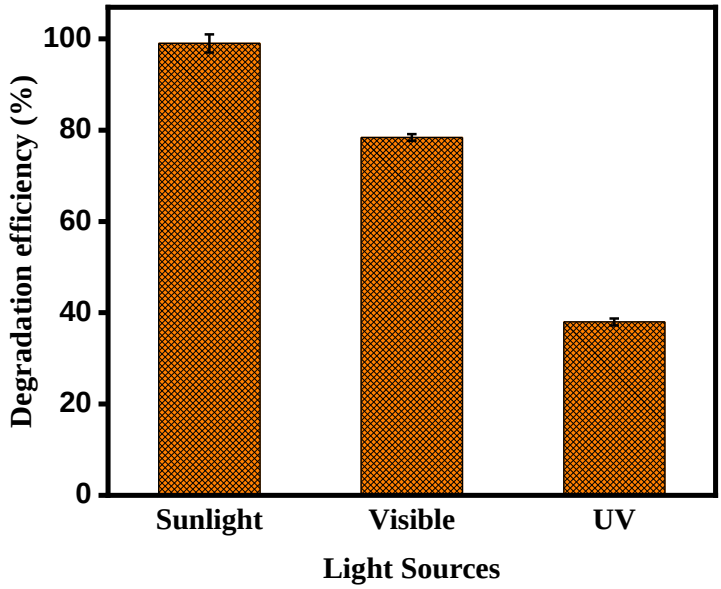

Figure 12 Changes in TC degradation induced by different light intensities employing a 13GS photocatalyst

3.2.10 Impact of solution pH

The degrading effectiveness of the photocatalyst is affected by the pH level of the TC solution, which in turn affects its capacity to adsorb contaminants on the composite surface[50]. To find

out how the pH of the solution affected the TC antibiotic elimination process, a range of solutions with varying pH levels were prepared using 0.1 N HCl and 0.1 N NaOH. The zero-charge state of the g-C_3N_4/Sb_2S_3 surface, denoted as pH_{pzc}, was found to be 6.93 (**Fig 13(a)**). TC being an amphoteric molecule has three acidity constants (pKa_1 = 3.30, pKa_2 = 7.7, and pKa_3 = 9.80). Each of TC's ionizing functional groups has a unique pKa value at a certain pH. TC is available as a cationic molecule (TCH_2^+ and TCH_3^+) when pH < 3.3 reason being the dimethyl ammonium group's protonation. When the tricarbonyl or the diketone group of phenol is deprotonated, it exists as an anionic species (TCH^- and TC_2^-) at a pH of around 7.7. Nevertheless, when the pH falls between 3.3 and 7.7, it takes on an amphoteric form (TCH±) as a result of the proton being removed from the phenol diketone group [51]. The efficiency of TC removal using the 13GS photocatalyst was diminished under acidic and alkaline environments, respectively, due to the electrostatic interactions between the cationic and anionic forms of TC and the positively and negatively charged surface of the photocatalyst. Electrostatic interaction between the zwitterionic pollutant and the negatively charged catalyst led to more effective degradation of the pharmaceutical pollutant TC. Therefore, the elimination of TC utilizing the 13GS composite was found to be maximum at a pH of 7 and showed greater efficacy in an alkaline environment compared to an acidic one as shown in **Fig 13(b)** [27].

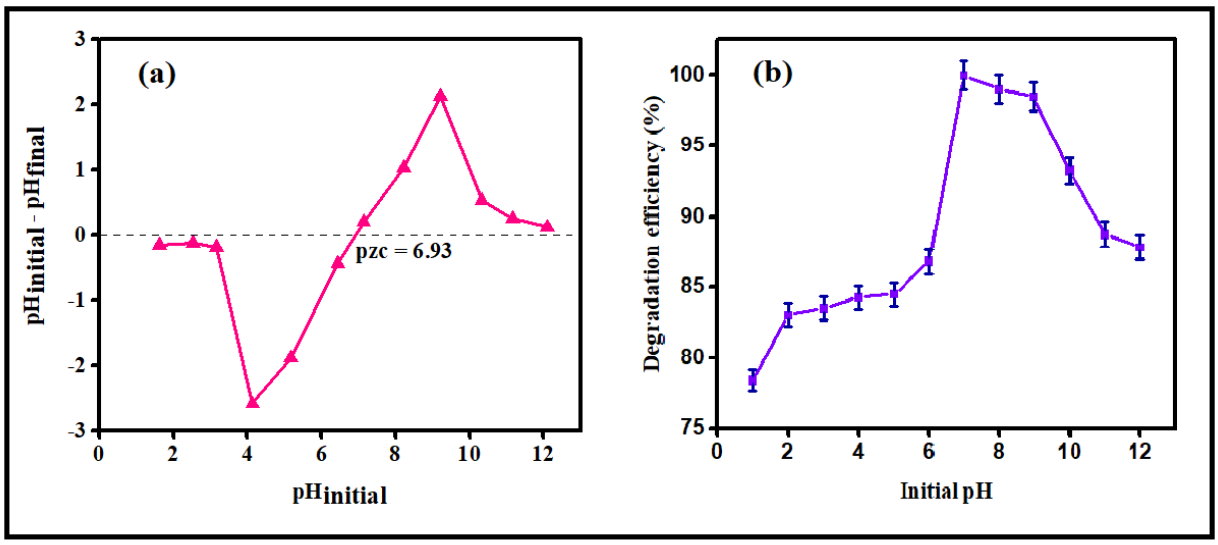

Figure 13 (a) Pzc of 13GS nanocomposite, (b) effect of pH on TC degradation

3.2.11 Reusability studies

In addition to its catalytic function, it is crucial to evaluate the durability of a photocatalyst for real-time applications. The repeatability and photostability of the 13GS photocatalyst were assessed by conducting consecutive recycling examinations. These studies aimed to analyze the photodegradation of TC under identical experimental circumstances where the catalyst underwent many cycles of photochemical reactions. Following each run, the catalyst underwent centrifugation, washing, and drying procedures before its utilization in the subsequent cycle. As shown in **Fig 14(a)** after six consecutive cycles of photocatalytic degradation, the degradation efficiency is still 80% which implies that 13GS is a reusable catalyst. The catalyst's inevitable loss during retrieval might explain the decrease in removal efficiency from 99% to 80%. Some untreated intermediates stuck to the catalyst's surface during the cycles may block pores and active sites and lower the performance. In addition, the sample (13GS) was examined for structural stability using XRD after six cycles (**Fig 14(b)**). Even after six cycles of usage, the photocatalyst crystal structure was visible in the XRD pattern, which revealed that the locations and intensities of typical diffraction peaks were stable and that no new diffraction peaks had emerged. In addition, FE-SEM examination verified that the composite's morphology was unaltered during the photo-catalytic degradation trials (**Fig 14(c)**). Based on the findings, the recently developed 13GS nanocomposite has exceptional stability and regeneration capabilities, making it a promising photocatalyst for use in a range of photocatalytic processes in the future.

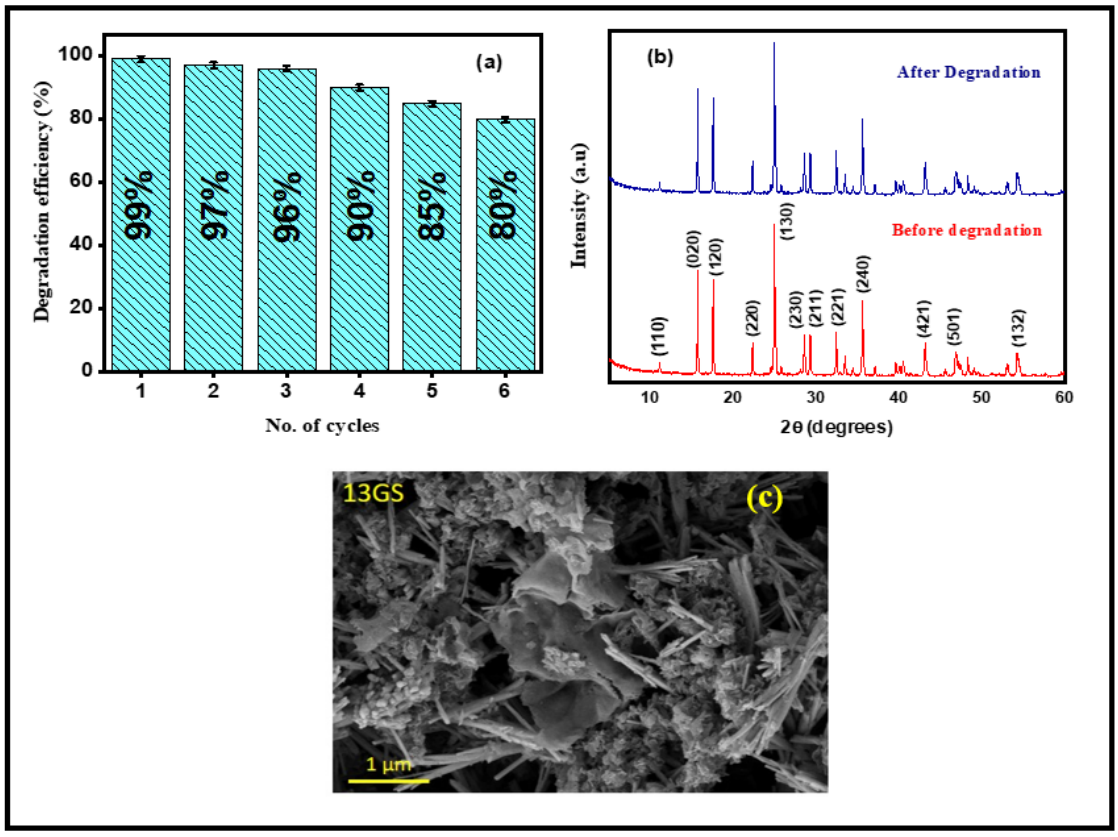

Figure 14 (a) Reusability graph, (b) XRD spectra of 13GS composite after photocatalytic use FE-SEM image of 13GS composite after photocatalytic usage

3.2.12 Mineralization studies

To assess the mineralization capacity of 13GS, TOC, and COD assessment experiments were conducted utilizing the titrimetric technique. The total organic carbon (TOC) and the chemical oxygen demand (COD) values were calculated using the provided **equations 5** and **6**, with pure water used as a reference sample.

$$\%TOC = \frac{TOC_i - TOC_f}{TOC_i} \times 100 \quad \textbf{(5)}$$

$$\%COD = \frac{COD_i - COD_f}{COD_i} \times 100 \quad \textbf{(6)}$$

Here, COD_i, COD_f, TOC_i, and TOC_f denote the starting and final values of COD and TOC, respectively. At first glance, the presence of elevated TOC and COD values suggested that the pollutant TC included a considerable quantity of organic compounds. Following a 120-minute exposure to sunshine, the TC compound exhibited reduction efficiencies of 89.5% for TOC and

68% for COD. TOC removal was lower than degradation due to the creation of sequential organic intermediate substances during the process. These substances were necessary for the full transformation of the targeted TC molecule into carbon dioxide and other simpler byproducts [27]. Natural medical/pharmaceutical wastewater could not be used for experiments due to restrictions imposed by ethical approvals. Based on the information provided in **Fig 15,** it can be inferred that the solutions underwent nearly full mineralization and included intermediates having a limited potential for mineralization. Our catalyst not only beats the previously published experiments but also shows remarkable efficacy as can be seen from the comparison of our work with theirs. Based on the findings of our research, the combination of g-C_3N_4 and Sb_2S_3 is an excellent choice.

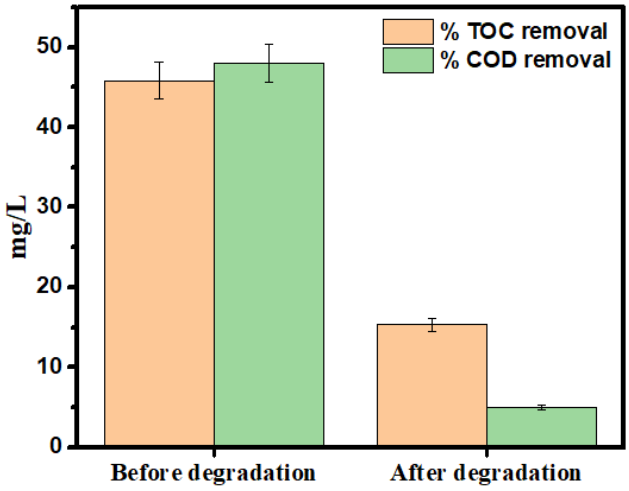

Figure 15 Analysis of TOC and COD levels before and after degradation

3.2.13 Scavenger impacts and a potential charge transfer pathway

Superoxide and hydroxyl radicals, as well as electrons in the conduction band (CB) and holes in the valence band (VB), are key players in the degradation process [19]. Scavenger research was carried out to identify the species that significantly contribute to the deterioration process. Hydroxyl radicals ($OH^{\cdot}$), electrons (e^{-}), superoxide radicals ($O_2{\cdot}^{-}$), and holes (h^{+}) were captured by several scavengers, including dimethyl sulfoxide (DMSO), isopropyl alcohol (IPA), benzoquinone, and methanol (CH_3OH), respectively [52]. Maximum degradation of 99% was shown by the TC in the absence of a trapping agent. However, adding those scavengers to the reaction mixture slowed down the photocatalytic degradation rate. **Fig 16** shows that the photocatalytic effectiveness of the 13GS composite was significantly affected by the addition of

DMSO. Based on these results, it seems that $OH^{\cdot}$ radicals were the main species responsible for the breakdown of TC. Just as h^+ plays a small but substantial part in removing the antibiotic, although to a lesser extent, the degradation process was also affected by the presence of methanol. The band gap values of pure GCN and SBS are calculated as 3.0 eV and 1.66 eV respectively [38][27]. The semiconductor's electrons moved from their valence bands to their conduction bands as they were exposed to light. To stop photo-generated charge carriers from reuniting, the presence of both semiconductors causes holes to move from the more positively charged valence band of GCN to the less positively charged valence band of SBS. In addition, electrons go from SBS's negatively charged conduction band to GCN's less negatively charged conduction band. The surface electrons on GCN can react with the O_2 molecules that have been dissolved, creating superoxide radical anions ($O_2^{\bullet-}$). These anions can then combine with water molecules to form hydroxide radicals ($OH^{\bullet}$). There are also protons in SBS's valence band that undergo a reaction with water, producing ($OH^{\cdot}$) hydroxide radicals. The oxidative species effectively break down TC, converting it into H_2O, CO_2, and other degradation products with reduced toxicity. This potential mechanism is depicted in the **scheme 2**. The likely reaction stages associated with the photocatalytic process are given in **equations 7-10**.

$$g\text{-}C_3N_4 / Sb_2S_3 + hv \rightarrow e^- + h^+ \quad \textbf{(7)}$$

$$e^-_{CB} + O_2 \rightarrow O_2^{\cdot -} \quad \textbf{(8)}$$

$$O_2^{\cdot -} + H_2O \rightarrow HOO^{\cdot} + OH^{\cdot} \quad \textbf{(9)}$$

$$h^+_{VB} + OH^- \rightarrow OH^{\cdot} \quad \textbf{(10)}$$

$$OH^{\cdot} / h^+ + \text{Pollutant} \rightarrow \text{Degraded products} \quad \textbf{(11)}$$

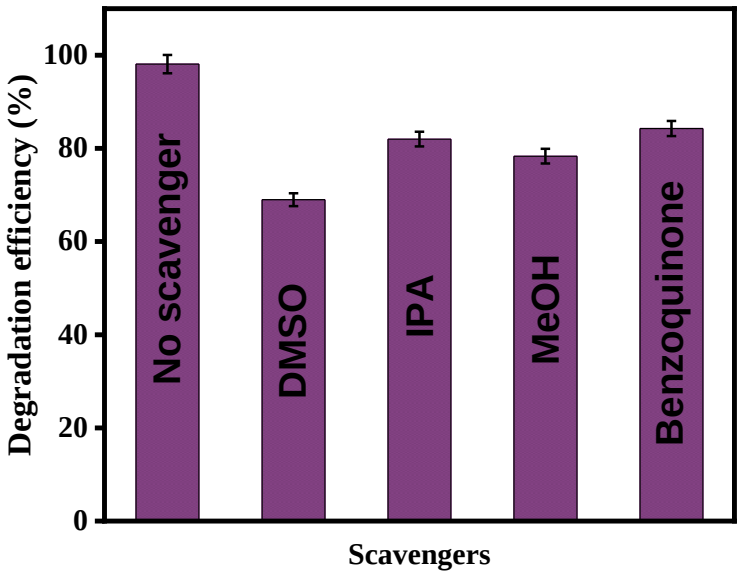

Figure 16 Effect of various scavengers on TC deterioration

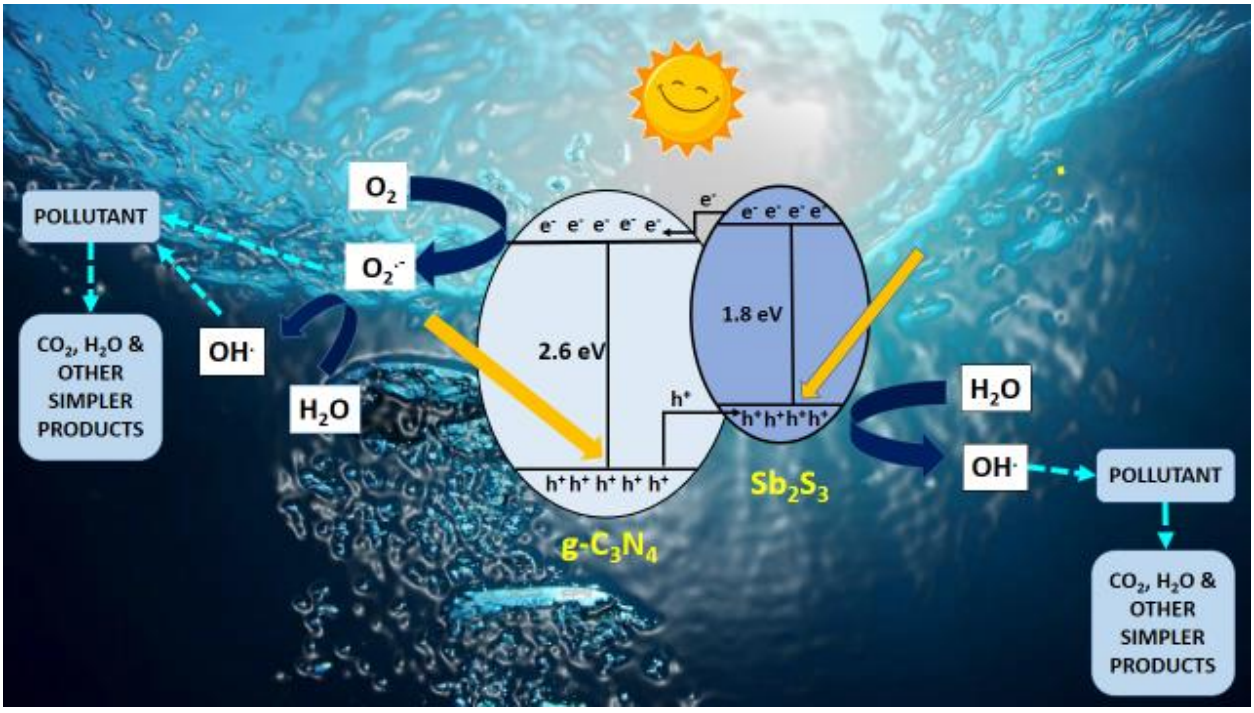

Scheme 2 The proposed route for the photodecomposition of contaminants by 13GS nanocomposite

CHAPTER 4 – CONCLUSION AND FUTURE SCOPE

Using the environment-friendly hydrothermal method, new heterojunction g-C_3N_4/Sb_2S_3 photocatalysts with different mole ratios were synthesized. Numerous analytical techniques, such as XRD, FE-SEM, EDS, XPS, UV-DRS, and BET analysis, were utilized to confirm the material's effective synthesis. FE-SEM analysis demonstrated that a heterojunction was efficiently produced when smaller SBS nanorods were placed onto bigger GCN nanosheets. To test how well the synthesized samples worked, they were subjected to natural sunlight for the photocatalytic breakdown of TC. The manufactured photocatalyst in terms of the rate constant, which is the highest was 13GS, which showed the greatest photocatalytic decomposition efficacy. The composite's low charge recombination rate and sufficient band gap allowed it to efficiently degrade the pollutants when exposed to natural sunshine, according to PL, BET, and UV-DRS examinations. Catalyst dose, pH studies, kinetics studies, the effect of various light sources, scavenger analysis, and reusability studies were some of the parameters that we investigated in our series of tests on photo-catalytic degradation. The primary factor affecting the pollutant's breakdown, as shown by trapping experiments, was $OH^{\cdot}$ Throughout six cycles, the composite's photocatalytic elimination of organic pollutants was remarkably effective. The results of the XRD and FE-SEM analyses showed that the TC physically adsorbed onto the composite, preserving its original properties. Our catalyst outperforms industry physicochemical approaches, as evidenced by higher percentages of COD and TOC removal. The photodegradation experiment’s byproducts and intermediates were investigated using GC-MS analysis. This study introduces g-C_3N_4/Sb_2S_3 as an innovative binary composite that has potential uses in a wide range of solar-driven processes.

These catalyst presents significant promise for addressing complex pollutants and treating industrial wastewater on a large scale. Their cost-effectiveness, ease of use, and environmental friendliness make them highly suitable for a range of wastewater treatment applications. By utilizing this catalyst, we can effectively combat the persistent accumulation of harmful toxic substances in aquatic systems. Its ability to provide a practical and sustainable solution highlights their potential to significantly improve water quality and protect environmental health.

References

[1] R. Gusain, K. Gupta, P. Joshi, and O. P. Khatri, ‘Adsorptive removal and photocatalytic degradation of organic pollutants using metal oxides and their composites: A comprehensive review’, *Adv. Colloid Interface Sci.*, vol. 272, p. 102009, Oct. 2019, doi: 10.1016/j.cis.2019.102009.

[2] T. Bekele Mekonnen, ‘An Overview on the Photocatalytic Degradation of Organic Pollutants in the Presence of Cerium Oxide (CeO₂) Based Nanoparticles: A Review’, *Nanosci. Nanometrology*, vol. 7, no. 1, p. 14, 2021, doi: 10.11648/j.nsnm.20210701.12.

[3] N. Pichel, M. Vivar, and M. Fuentes, ‘The problem of drinking water access: A review of disinfection technologies with an emphasis on solar treatment methods’, *Chemosphere*, vol. 218, pp. 1014–1030, Mar. 2019, doi: 10.1016/j.chemosphere.2018.11.205.

[4] S. Singla, P. Singh, S. Basu, and P. Devi, ‘BiVO4/MoSe2 Photocatalyst for the photocatalytic Abatement of tetracycline and photoelectrocatalytic water splitting’, *Mater. Chem. Phys.*, vol. 295, p. 127111, Feb. 2023, doi: 10.1016/j.matchemphys.2022.127111.

[5] R. A. Palominos, M. A. Mondaca, A. Giraldo, G. Peñuela, M. Pérez-Moya, and H. D. Mansilla, ‘Photocatalytic oxidation of the antibiotic tetracycline on TiO2 and ZnO suspensions’, *Catal. Today*, vol. 144, no. 1–2, pp. 100–105, Jun. 2009, doi: 10.1016/j.cattod.2008.12.031.

[6] F. Ahmad, D. Zhu, and J. Sun, ‘Environmental fate of tetracycline antibiotics: degradation pathway mechanisms, challenges, and perspectives’, *Environ. Sci. Eur.*, vol. 33, no. 1, p. 64, Dec. 2021, doi: 10.1186/s12302-021-00505-y.

[7] M. Addamo *et al.*, ‘Removal of drugs in aqueous systems by photoassisted degradation’, *J. Appl. Electrochem.*, vol. 35, no. 7–8, pp. 765–774, Jul. 2005, doi: 10.1007/s10800-005-1630-y.

[8] J. Guo *et al.*, ‘Photocatalytic degradation of tetracycline antibiotics using delafossite silver ferrite-based Z-scheme photocatalyst: Pathways and mechanism insight’, *Chemosphere*, vol. 270, p. 128651, May 2021, doi: 10.1016/j.chemosphere.2020.128651.

[9] P. Zhang, Y. Li, Y. Cao, and L. Han, 'Characteristics of tetracycline adsorption by cow manure biochar prepared at different pyrolysis temperatures', *Bioresour. Technol.*, vol. 285, p. 121348, Aug. 2019, doi: 10.1016/j.biortech.2019.121348.

[10] I. C. Iakovides *et al.*, 'Continuous ozonation of urban wastewater: Removal of antibiotics, antibiotic-resistant Escherichia coli and antibiotic resistance genes and phytotoxicity', *Water Res.*, vol. 159, pp. 333–347, Aug. 2019, doi: 10.1016/j.watres.2019.05.025.

[11] A. M. Cahino, M. M. A. de Andrade, E. S. de Araújo, E. L. Silva, C. de O. Cunha, and E. M. R. Rocha, 'Degradation of tetracycline by solar photo-Fenton: Optimization and application in pilot photoreactor', *Environ. Qual. Manag.*, vol. 28, no. 1, pp. 101–106, Sep. 2018, doi: 10.1002/tqem.21579.

[12] J. Wang, D. Zhi, H. Zhou, X. He, and D. Zhang, 'Evaluating tetracycline degradation pathway and intermediate toxicity during the electrochemical oxidation over a Ti/Ti4O7 anode', *Water Res.*, vol. 137, pp. 324–334, Jun. 2018, doi: 10.1016/j.watres.2018.03.030.

[13] X. Wen *et al.*, 'Immobilized laccase on bentonite-derived mesoporous materials for removal of tetracycline', *Chemosphere*, vol. 222, pp. 865–871, May 2019, doi: 10.1016/j.chemosphere.2019.02.020.

[14] G. Yang, D. Bao, D. Zhang, C. Wang, L. Qu, and H. Li, 'Removal of Antibiotics From Water with an All-Carbon 3D Nanofiltration Membrane', *Nanoscale Res. Lett.*, vol. 13, no. 1, p. 146, Dec. 2018, doi: 10.1186/s11671-018-2555-9.

[15] J. Hou *et al.*, 'Simultaneous removal of antibiotics and antibiotic resistance genes from pharmaceutical wastewater using the combinations of up-flow anaerobic sludge bed, anoxic-oxic tank, and advanced oxidation technologies', *Water Res.*, vol. 159, pp. 511–520, Aug. 2019, doi: 10.1016/j.watres.2019.05.034.

[16] H. Wang *et al.*, 'Visible-light-driven removal of tetracycline antibiotics and reclamation of hydrogen energy from natural water matrices and wastewater by polymeric carbon nitride foam', *Water Res.*, vol. 144, pp. 215–225, Nov. 2018, doi: 10.1016/j.watres.2018.07.025.

[17] I. A. Vasiliadou, R. Molina, M. I. Pariente, K. C. Christoforidis, F. Martinez, and J. A. Melero, 'Understanding the role of mediators in the efficiency of advanced oxidation

processes using white-rot fungi', *Chem. Eng. J.*, vol. 359, pp. 1427–1435, Mar. 2019, doi: 10.1016/j.cej.2018.11.035.

[18] H. Xiong, S. Dong, J. Zhang, D. Zhou, and B. E. Rittmann, 'Roles of an easily biodegradable co-substrate in enhancing tetracycline treatment in an intimately coupled photocatalytic-biological reactor', *Water Res.*, vol. 136, pp. 75–83, Jun. 2018, doi: 10.1016/j.watres.2018.02.061.

[19] A. Kundu, S. Sharma, and S. Basu, 'Modulated BiOCl nanoplates with porous g-C3N4 nanosheets for photocatalytic degradation of color/colorless pollutants in natural sunlight', *J. Phys. Chem. Solids*, vol. 154, p. 110064, Jul. 2021, doi: 10.1016/j.jpcs.2021.110064.

[20] B. Li and T. Zhang, 'Biodegradation and Adsorption of Antibiotics in the Activated Sludge Process', *Environ. Sci. Technol.*, vol. 44, no. 9, pp. 3468–3473, May 2010, doi: 10.1021/es903490h.

[21] Y. He, W. Sang, W. Lu, W. Zhang, C. Zhan, and D. Jia, 'Recent Advances of Emerging Organic Pollutants Degradation in Environment by Non-Thermal Plasma Technology: A Review', *Water*, vol. 14, no. 9, p. 1351, Apr. 2022, doi: 10.3390/w14091351.

[22] A. Mishra, A. Mehta, S. Basu, N. P. Shetti, K. R. Reddy, and T. M. Aminabhavi, 'Graphitic carbon nitride (g–C3N4)–based metal-free photocatalysts for water splitting: A review', *Carbon N. Y.*, vol. 149, pp. 693–721, Aug. 2019, doi: 10.1016/j.carbon.2019.04.104.

[23] A. Mishra, S. Basu, N. P. Shetti, K. R. Reddy, and T. M. Aminabhavi, 'Photocatalysis of Graphene and Carbon Nitride-Based Functional Carbon Quantum Dots', in *Nanoscale Materials in Water Purification*, Elsevier, 2019, pp. 759–781. doi: 10.1016/B978-0-12-813926-4.00035-5.

[24] L. Sun *et al.*, 'Enhanced Visible-Light Photocatalytic Activity of BiOI/BiOCl Heterojunctions: Key Role of Crystal Facet Combination', *ACS Catal.*, vol. 5, no. 6, pp. 3540–3551, Jun. 2015, doi: 10.1021/cs501631n.

[25] S. Cao and J. Yu, 'g-C 3 N 4 -Based Photocatalysts for Hydrogen Generation', *J. Phys. Chem. Lett.*, vol. 5, no. 12, pp. 2101–2107, Jun. 2014, doi: 10.1021/jz500546b.

[26] R. Makhloufi, S. E. Hachani, A. Fettah, W. Tair, and Z. Zekri, ‘Synthesis of Sb2S3-Sb4O5Cl2 composite used as a photocatalyst for crystal violet cationic dye degradation’, *Chem. Data Collect.*, vol. 39, p. 100867, Jun. 2022, doi: 10.1016/j.cdc.2022.100867.

[27] S. Singla, P. Devi, and S. Basu, ‘Highly Effectual Photocatalytic Remediation of Tetracycline under the Broad Spectrum of Sunlight by Novel BiVO4/Sb2S3 Nanocomposite’, *Catalysts*, vol. 13, no. 4, p. 731, Apr. 2023, doi: 10.3390/catal13040731.

[28] C. Ayappan, V. Jayaraman, B. Palanivel, A. Pandikumar, and A. Mani, ‘Facile preparation of novel Sb2S3 nanoparticles/rod-like α-Ag2WO4 heterojunction photocatalysts: Continuous modulation of band structure towards the efficient removal of organic contaminants’, *Sep. Purif. Technol.*, vol. 236, p. 116302, Apr. 2020, doi: 10.1016/j.seppur.2019.116302.

[29] L. Dashairya, S. Sharma, A. Rathi, P. Saha, and S. Basu, ‘Solar-light-driven photocatalysis by Sb2S3/carbon based composites towards degradation of noxious organic pollutants’, *Mater. Chem. Phys.*, vol. 273, p. 125120, Nov. 2021, doi: 10.1016/j.matchemphys.2021.125120.

[30] W. Peng and X. Li, ‘Synthesis of MoS2/g-C3N4 as a solar light-responsive photocatalyst for organic degradation’, *Catal. Commun.*, vol. 49, pp. 63–67, Apr. 2014, doi: 10.1016/j.catcom.2014.02.008.

[31] J. Meng *et al.*, ‘Facile synthesis of g-C 3 N 4 nanosheets loaded with WO 3 nanoparticles with enhanced photocatalytic performance under visible light irradiation’, *RSC Adv.*, vol. 7, no. 39, pp. 24097–24104, 2017, doi: 10.1039/C7RA02297B.

[32] A. K. Berekute, K.-P. Yu, Y.-H. Chuang, and K.-Y. Lin, ‘Novel visible-light-induced P-doped g-C3N4/α-Bi2O3 nanocomposite photocatalysts for enhanced degradation of refractory endocrine disruptors—benzophenones’, *Appl. Surf. Sci.*, vol. 607, p. 154987, Jan. 2023, doi: 10.1016/j.apsusc.2022.154987.

[33] Y. Xiao *et al.*, ‘Hierarchical Sb2S3/ZnIn2S4 core–shell heterostructure for highly efficient photocatalytic hydrogen production and pollutant degradation’, *J. Colloid Interface Sci.*, vol. 623, pp. 109–123, Oct. 2022, doi: 10.1016/j.jcis.2022.04.137.

[34] X. Wang, M. Hong, F. Zhang, Z. Zhuang, and Y. Yu, 'Recyclable Nanoscale Zero Valent Iron Doped g-C 3 N 4 /MoS 2 for Efficient Photocatalysis of RhB and Cr(VI) Driven by Visible Light', *ACS Sustain. Chem. Eng.*, vol. 4, no. 7, pp. 4055–4063, Jul. 2016, doi: 10.1021/acssuschemeng.6b01024.

[35] L. Shi, T. Yu, and T. Q. Bui, 'Numerical Modelling of Hydraulic Fracturing in Rock Mass by Xfem', *Soil Mech. Found. Eng.*, vol. 52, no. 2, pp. 74–83, May 2015, doi: 10.1007/s11204-015-9309-9.

[36] H. M. El-Bery, M. R. Salah, S. M. Ahmed, and S. A. Soliman, 'Efficient non-metal based conducting polymers for photocatalytic hydrogen production: comparative study between polyaniline, polypyrrole and PEDOT', *RSC Adv.*, vol. 11, no. 22, pp. 13229–13244, 2021, doi: 10.1039/D1RA01218E.

[37] J. Kröger *et al.*, 'Interfacial Engineering for Improved Photocatalysis in a Charge Storing 2D Carbon Nitride: Melamine Functionalized Poly(heptazine imide)', *Adv. Energy Mater.*, vol. 11, no. 6, Feb. 2021, doi: 10.1002/aenm.202003016.

[38] D. Monga, D. Ilager, N. P. Shetti, S. Basu, and T. M. Aminabhavi, '2D/2d heterojunction of MoS2/g-C3N4 nanoflowers for enhanced visible-light-driven photocatalytic and electrochemical degradation of organic pollutants', *J. Environ. Manage.*, vol. 274, p. 111208, Nov. 2020, doi: 10.1016/j.jenvman.2020.111208.

[39] Y. Cui *et al.*, 'Synthesis of bulk and nanoporous carbon nitride polymers from ammonium thiocyanate for photocatalytic hydrogen evolution', *J. Mater. Chem.*, vol. 21, no. 34, p. 13032, 2011, doi: 10.1039/c1jm11961c.

[40] V. N. Khabashesku, J. L. Zimmerman, and J. L. Margrave, 'Powder Synthesis and Characterization of Amorphous Carbon Nitride', *Chem. Mater.*, vol. 12, no. 11, pp. 3264–3270, Nov. 2000, doi: 10.1021/cm000328r.

[41] Z. Huang, Q. Sun, K. Lv, Z. Zhang, M. Li, and B. Li, 'Effect of contact interface between TiO2 and g-C3N4 on the photoreactivity of g-C3N4/TiO2 photocatalyst: (0 0 1) vs (1 0 1) facets of TiO2', *Appl. Catal. B Environ.*, vol. 164, pp. 420–427, Mar. 2015, doi: 10.1016/j.apcatb.2014.09.043.

[42] W. Luo *et al.*, ‘Imbedding ultrafine Sb2S3 nanoparticles in mesoporous carbon sphere for high-performance lithium-ion battery’, *Electrochim. Acta*, vol. 290, pp. 185–192, Nov. 2018, doi: 10.1016/j.electacta.2018.09.070.

[43] L. Tan *et al.*, ‘Sb2Se3 assembling Sb2O3@ attapulgite as an emerging composites for catalytic hydrogenation of p-nitrophenol’, *Sci. Rep.*, vol. 7, no. 1, p. 3281, Jun. 2017, doi: 10.1038/s41598-017-03281-z.

[44] J. Grigas, E. Talik, and V. Lazauskas, ‘X-ray Photoelectron Spectroscopy of Sb 2 S 3 Crystals’, *Phase Transitions*, vol. 75, no. 3, pp. 323–337, Jan. 2002, doi: 10.1080/01411590290020448.

[45] L. Gnanasekaran *et al.*, ‘Nanosized Fe3O4 incorporated on a TiO2 surface for the enhanced photocatalytic degradation of organic pollutants’, *J. Mol. Liq.*, vol. 287, p. 110967, Aug. 2019, doi: 10.1016/j.molliq.2019.110967.

[46] F. Hasanvandian, M. Moradi, S. Aghaebrahimi Samani, B. Kakavandi, S. Rahman Setayesh, and M. Noorisepehr, ‘Effective promotion of g–C3N4 photocatalytic performance via surface oxygen vacancy and coupling with bismuth-based semiconductors towards antibiotics degradation’, *Chemosphere*, vol. 287, p. 132273, Jan. 2022, doi: 10.1016/j.chemosphere.2021.132273.

[47] L. Zhang *et al.*, ‘Photocatalytic degradation of rhodamine B by Bi2O3@LDHs S–scheme heterojunction: Performance, kinetics and mechanism’, *Appl. Surf. Sci.*, vol. 567, p. 150760, Nov. 2021, doi: 10.1016/j.apsusc.2021.150760.

[48] S. Kumar, T. Surendar, A. Baruah, and V. Shanker, ‘Synthesis of a novel and stable g-C3N4–Ag3PO4 hybrid nanocomposite photocatalyst and study of the photocatalytic activity under visible light irradiation’, *J. Mater. Chem. A*, vol. 1, no. 17, p. 5333, 2013, doi: 10.1039/c3ta00186e.

[49] D. Monga and S. Basu, ‘Enhanced photocatalytic degradation of industrial dye by g-C3N4/TiO2 nanocomposite: Role of shape of TiO2’, *Adv. Powder Technol.*, vol. 30, no. 5, pp. 1089–1098, May 2019, doi: 10.1016/j.apt.2019.03.004.

[50] A. Kumar, R. Kumar, and G. Pandey, ‘Synthesis, Characterization of

Titania/Polyaniline/GO Nanocomposites, and Its Photocatalytic Activity Under UV-Visible Light', *Macromol. Symp.*, vol. 379, no. 1, Jun. 2018, doi: 10.1002/masy.201600192.

[51] X. Wang, J. Jia, and Y. Wang, 'Combination of photocatalysis with hydrodynamic cavitation for degradation of tetracycline', *Chem. Eng. J.*, vol. 315, pp. 274–282, May 2017, doi: 10.1016/j.cej.2017.01.011.

[52] S. Singla, S. Sharma, and S. Basu, 'MoS2/WO3 heterojunction with the intensified photocatalytic performance for decomposition of organic pollutants under the broad array of solar light', *J. Clean. Prod.*, vol. 324, p. 129290, Nov. 2021, doi: 10.1016/j.jclepro.2021.129290.

DCBC File100

ORIGINALITY REPORT

17%	12%	14%	4%
SIMILARITY INDEX	INTERNET SOURCES	PUBLICATIONS	STUDENT PAPERS

PRIMARY SOURCES

1	Aanchal Rathi, Soumen Basu, Sanghamitra Barman. "Adsorptive removal of fipronil from its aqueous solution by modified zeolite HZSM-5: Equilibrium, kinetic and thermodynamic study", Journal of Molecular Liquids, 2019 Publication	2%
2	www.tandfonline.com Internet Source	1%
3	Charu Maggu, Shelly Singla, Soumen Basu. "Unleashing the power of sunlight: Bi2O3/Sb2S3 photocatalysis for sustainable wastewater remediation of Tetracycline and Rhodamine-B", Journal of Environmental Management, 2024 Publication	1%
4	www.science.gov Internet Source	1%
5	Pritam Hait, Rajeev Mehta, Soumen Basu. "Advancing sustainable solutions: Harnessing polyaniline/BiOCl/GO ternary nanocomposites	<1%

for solar-powered degradation of organic pollutant and photocatalytic hydrogen generation", Journal of Cleaner Production, 2023
Publication

6	Wee-Jun Ong, Lling-Lling Tan, Yun Hau Ng, Siek-Ting Yong, Siang-Piao Chai. " Graphitic Carbon Nitride (g-C N)-Based Photocatalysts for Artificial Photosynthesis and Environmental Remediation: Are We a Step Closer To Achieving Sustainability? ", Chemical Reviews, 2016 Publication	<1 %
7	www.scribd.com Internet Source	<1 %
8	coek.info Internet Source	<1 %
9	www.researchgate.net Internet Source	<1 %
10	espace.curtin.edu.au Internet Source	<1 %
11	link.springer.com Internet Source	<1 %
12	Jabbari, V., J.M. Veleta, M. Zarei-Chaleshtori, J. Gardea-Torresdey, and D. Villagrán. "Green synthesis of magnetic MOF@GO and	<1 %

MOF@CNT hybrid nanocomposites with high adsorption capacity towards organic pollutants", Chemical Engineering Journal, 2016.
Publication

---

13 Wang, Hui, Xingzhong Yuan, Hou Wang, Xiaohong Chen, Zhibin Wu, Longbo Jiang, Weiping Xiong, and Guangming Zeng. "Facile synthesis of Sb2S3/ultrathin g-C3N4 sheets heterostructures embedded with g-C3N4 quantum dots with enhanced NIR-light photocatalytic performance", Applied Catalysis B Environmental, 2016.
Publication

<1 %

---

14 vdoc.pub
Internet Source

<1 %

---

15 Peixun Xiong, Junxiu Wu, Mengfan Zhou, Yunhua Xu. "Bismuth–Antimony Alloy Nanoparticle@Porous Carbon Nanosheet Composite Anode for High-Performance Potassium-Ion Batteries", ACS Nano, 2019
Publication

<1 %

---

16 ethesisarchive.library.tu.ac.th
Internet Source

<1 %

---

17 purehost.bath.ac.uk
Internet Source

<1 %

---

18 www.researchsquare.com
Internet Source

		<1%
19	wiredspace.wits.ac.za Internet Source	<1%
20	Submitted to Higher Education Commission Pakistan Student Paper	<1%
21	Neelam Kumar, Naveen Chandra Joshi. "Adsorption applications of synthetically prepared PANI-CuO based nanocomposite material", Journal of the Indian Chemical Society, 2022 Publication	<1%
22	iris.unito.it Internet Source	<1%
23	dns2.asia.edu.tw Internet Source	<1%
24	eprints.qut.edu.au Internet Source	<1%
25	Cun Li, Xiaogang Yang, Baojun Yang, Yan Yan, Yitai Qian. "Synthesis and characterization of nitrogen-rich graphitic carbon nitride", Materials Chemistry and Physics, 2007 Publication	<1%
26	studylib.net Internet Source	<1%

27	www2.mdpi.com Internet Source	<1%
28	Heng Liu, Wanqiang Liu, Yan Sun, Peng Chen, Jianxun Zhao, Xin Guo, Zhongmin Su. "Preparation and electrochemical hydrogen storage properties of Ti49Zr26Ni25 alloy covered with porous polyaniline", International Journal of Hydrogen Energy, 2020 Publication	<1%
29	Submitted to King's College Student Paper	<1%
30	Gabriela Ciobanu, Simona Barna, Maria Harja. "Kinetic and equilibrium studies on adsorption of Reactive Blue 19 dye from aqueous solutions by nanohydroxyapatite adsorbent", Archives of Environmental Protection, 2016 Publication	<1%
31	hdl.handle.net Internet Source	<1%
32	lutpub.lut.fi Internet Source	<1%
33	S. K. Mehta, J. P. Gaur. "Use of Algae for Removing Heavy Metal Ions From Wastewater: Progress and Prospects", Critical Reviews in Biotechnology, 2008 Publication	<1%

34	Submitted to Universiti Teknologi Malaysia Student Paper	<1 %
35	docksci.com Internet Source	<1 %
36	etd.cput.ac.za Internet Source	<1 %
37	Submitted to University of Wales Swansea Student Paper	<1 %
38	jhs.mazums.ac.ir Internet Source	<1 %
39	repositorio.ucam.edu Internet Source	<1 %
40	Peisheng Guo, Huawei Song, Yuyi Liu, Chengxin Wang. "FeNi 2 S 4 QDs @C composites as a high capacity and long life anode material for lithium ion battery and ex situ investigation of electrochemical mechanism", Electrochimica Acta, 2017 Publication	<1 %
41	core.ac.uk Internet Source	<1 %
42	pubs.rsc.org Internet Source	<1 %
43	www.ajnanomat.com Internet Source	<1 %

44	www.freepatentsonline.com Internet Source	<1 %
45	Jhih-Ci Yang. "Assessment of adequate sodium hypochlorite concentration for pre-oxidization of multi-walled carbon nanotubes", Journal of Chemical Technology & Biotechnology, 2010 Publication	<1 %
46	Submitted to University of Babylon Student Paper	<1 %
47	arizona.openrepository.com Internet Source	<1 %
48	pure.mpg.de Internet Source	<1 %
49	www.scirp.org Internet Source	<1 %
50	www.trademarkelite.com Internet Source	<1 %
51	Ozer, D.. "Methylene blue adsorption from aqueous solution by dehydrated peanut hull", Journal of Hazardous Materials, 20070601 Publication	<1 %
52	Wang, Xinpeng, Zhiming Liu, Huiqing Zhong, Jianfeng Yu, Mei Jin, and Zhouyi Guo. "A facile one-step approach to functionalized graphene oxide-based hydrogels used as	<1 %

effective adsorbents toward anionic dyes", Applied Surface Science, 2014.
Publication

53	pure.hw.ac.uk Internet Source	<1%
54	www.cgwb.gov.in Internet Source	<1%
55	Bharat C. Choudhary, Debajyoti Paul, Amulrao U. Borse, Dipak J. Garole. "Surface functionalized biomass for adsorption and recovery of gold from electronic scrap and refinery wastewater", Separation and Purification Technology, 2018 Publication	<1%
56	Ruonan Guo, Xinyu Qi, Xinyi Zhang, Huixuan Zhang, Xiuwen Cheng. "Synthesis of Ag2CO3/α-Fe2O3 heterojunction and it high visible light driven photocatalytic activity for elimination of organic pollutants", Separation and Purification Technology, 2018 Publication	<1%
57	Yan, Tingsong, Xuegang Luo, Xiaoyan Lin, and Jiayi Yang. "Preparation, characterization and adsorption properties for lead (II) of alkali-activated porous leather particles", Colloids and Surfaces A Physicochemical and Engineering Aspects, 2017. Publication	<1%

58	Yung-Tse Hung. "Batch adsorption of organic pollutants from oxidation pond effluents using fly ashes", International Journal of Environmental Studies, 2007 Publication	<1 %
59	mdpi-res.com Internet Source	<1 %
60	www.research-collection.ethz.ch Internet Source	<1 %
61	Ana L. Cukierman, Ana L. Cukierman, Ana L. Cukierman, Pablo R. Bonelli, Pablo R. Bonelli. "Capture of Water Contaminants by a New Generation of Sorbents Based on Graphene and Related Materials", Wiley, 2018 Publication	<1 %
62	Submitted to Heriot-Watt University Student Paper	<1 %
63	Shuangzhen Guo, Kaili Wu, Yan Gao, Lihua Liu, Xixi Zhu, Xianlong Li, Fan Zhang. "Efficient Removal of Zn(II), Pb(II), and Cd(II) in Waste Water Based on Magnetic Graphitic Carbon Nitride Materials with Enhanced Adsorption Capacity", Journal of Chemical & Engineering Data, 2018 Publication	<1 %
64	assets-eu.researchsquare.com Internet Source	<1 %

65	cyberleninka.org Internet Source	<1 %
66	tudr.thapar.edu:8080 Internet Source	<1 %
67	A. Malathi, Prabhakarn Arunachalam, Andrews Nirmala Grace, J. Madhavan, Abdullah M. Al-Mayouf. "A robust visible-light driven BiFeWO 6 /BiOI nanohybrid with efficient photocatalytic and photoelectrochemical performance", Applied Surface Science, 2017 Publication	<1 %
68	Xue-Song Wang, Hai-Qiong Hu, Cheng Sun. "Removal of Copper (II) Ions from Aqueous Solutions using Na-mordenite", Separation Science and Technology, 2007 Publication	<1 %
69	asianpubs.org Internet Source	<1 %
70	escholarship.mcgill.ca Internet Source	<1 %
71	patents.google.com Internet Source	<1 %
72	studentsrepo.um.edu.my Internet Source	<1 %
	www.iosrjournals.org	

73	Internet Source	<1%
74	ArchanaA. Biradar. "Entrapping Flavin-Containing Monooxygenase on Corrugated Silica Nanospheres and their Recyclable Biocatalytic Activities", ChemCatChem, 03/24/2010 Publication	<1%
75	Submitted to Coventry University Student Paper	<1%
76	Gupta, S.S.. "Adsorption of Ni(II) on clays", Journal of Colloid And Interface Science, 20060301 Publication	<1%
77	Submitted to Imperial College of Science, Technology and Medicine Student Paper	<1%
78	discovery.researcher.life Internet Source	<1%
79	munin.uit.no Internet Source	<1%
80	ourspace.uregina.ca Internet Source	<1%
81	Chalida Niamnuy, Sirada Sungsinchai, Prapaporn Jarernsamrit, Sakamon Devahastin, Metta Chareonpanich. "Synthesis	<1%

and characterization of aluminosilicate and zinc silicate from sugarcane bagasse fly ash for adsorption of aflatoxin B1", Scientific Reports, 2024
Publication

---

82 Isah A., Umar, Giwa Abdulraheem, Salisu Bala, Sallahudeen Muhammad, and Mustapha Abdullahi. "Kinetics, equilibrium and thermodynamics studies of C.I. Reactive Blue 19 dye adsorption on coconut shell based activated carbon", International Biodeterioration & Biodegradation, 2015. <1 %
Publication

---

83 Subramanyam, B.. "Study of the adsorption of phenol by two soils based on kinetic and isotherm modeling analyses", Desalination, 20091225 <1 %
Publication

---

84 Taleb, Khaled. "Application of Macroporous Resin and Cellulose Based Materials Modified with Iron Oxides for Arsenic Removal", University of Belgrade (Serbia), 2024 <1 %
Publication

---

85 Tarab Fatima, Samina Husain, Manika Khanuja. "Novel ternary Z scheme carbon quantum dots (CQDs) decorated WS2/PANI ((CQDs@WS2/PANI):0D:2D:1D) nanocomposite for the photocatalytic <1 %

degradation and electrochemical detection of pharmaceutical drugs", Nano Materials Science, 2024
Publication

86	Wang, Sui, Jing Wei, Shasha Lv, Zhiyong Guo, and Feng Jiang. "Removal of organic dyes in environmental water onto magnetic-sulfonic graphene nanocomposite", CLEAN - Soil Air Water, 2013. Publication	<1 %
87	Xuedong Ma, Yajie Cao, Jie Deng, Jiatang Shao, Xiaoyun Feng, Weiqi Li, Shuang Li, Riguang Zhang. "Synergistic enhancement of N, S co-modified biochar for removal of tetracycline hydrochloride from aqueous solution: Tunable micro-mesoporosity and chemisorption sites", Chemical Engineering Journal, 2024 Publication	<1 %
88	acikerisim.erdogan.edu.tr Internet Source	<1 %
89	crimsonpublishers.com Internet Source	<1 %
90	dspace.uef.fi Internet Source	<1 %
91	fdocumentos.tips Internet Source	<1 %

92	fse.studenttheses.ub.rug.nl Internet Source	<1 %
93	kb.psu.ac.th:8080 Internet Source	<1 %
94	kipdf.com Internet Source	<1 %
95	nopr.niscpr.res.in Internet Source	<1 %
96	periodicos.ufpb.br Internet Source	<1 %
97	public.thinkonweb.com Internet Source	<1 %
98	smartech.gatech.edu Internet Source	<1 %
99	www.frontiersin.org Internet Source	<1 %
100	www.lifesciencesite.com Internet Source	<1 %
101	www.peeref.com Internet Source	<1 %
102	www.slideshare.net Internet Source	<1 %
103	Monika Duhan, Raminder Kaur. "Adsorptive removal of methyl orange with polyaniline	<1 %

nanofibers: an unconventional adsorbent for water treatment", Environmental Technology, 2019
Publication

104 Igberase, Ephraim. "The Adsorption of Cu(II) Ions by Polyaniline Grafted Chitosan Beads", Vaal University of Technology (South Africa), 2024 <1%
Publication

105 Jing Yang, Li Li Ma, Bin Shen, Jian Hua Zhu. "Capturing Nitrosamines in Environment by Zeolite", Materials and Manufacturing Processes, 2007 <1%
Publication

106 (10-25-13) http://204.64.181.50/innovativewater/desal/projects/ut <1%
Internet Source

Exclude quotes	On	Exclude matches	Off
Exclude bibliography	On